CHAPTER *6*
INTERPRETATION OF THE OBSERVED LINES

6.1 <u>GENERAL</u> <u>CONSIDERATIONS:</u>

The ionized gas responsible for the observed recombination lines is characterized by several parameters. Some of these are

1. The electron temperature
2. The electron density
3. The size of the line emitting region
4. The emission measure $= \int_o^L N_e^2 \, dL$ which combines the extent of the gas along the line of sight and the square of the electron density
5. Clumpiness of gas which can be characterized by the the filling factor f of the gas in a given volume.
6. Microturbulence which contributes to the width of the line, and which can be characterized by the rms turbulent velocity $\langle V_t^2 \rangle^{1/2}$.

There can be variation of one or more of these parameters over the line emitting region. For a complete description of the gas which produces the observed lines, one should determine all of these parameters. The aim of any recombination line observation is to get a handle on one or more of these parameters and to see the manifestation of interesting physical processes like pressure broadening and stimulated emission which are expected to play a part in the formation of these lines. In this chapter, we will make use of the theory of recombination line formation, outlined in Chapter 2, and derive some of the properties of the regions

responsible for the observed lines using the line parameters presented in chapter 5.

The detection of a recombination line in a given direction essentially yields the following **3** line parameters for every line component

1. the peak line intensity $T_L (^oK)$
2. the full line width at half intensity $\Delta V(kms^{-1})$
3. **the line centre velocity** $V_{LSR} (kms^{-1})$

In addition, the average continuum beam brightness temperature T_{BC} is also measured in the same direction. The last of the three line parameters (V_{LSR}) relates only to the overall motion of the source along the line of sight which in turn can indicate the position of the source if a model of galactic rotation is used. This parameter therefore, cannot be used to derive or put constraints on any of the physical properties of the line emitting region. We are then left with only three observed quantities T_L , ΔV and T_{BC} , which is much fewer than the number of parameters which characterize the line emitting region. Further, at the frequency of our observation, only the line intensity T_L and the width ΔV are directly related to the source parameters. The total continuum temperature T_{BC} is dominated by the non-thermal galactic background, unlike at high frequencies (>few **GHz**) where the continuum is mostly thermal radiation from the line emitting region itself. This being so, **it** is not possible at this frequency to use the ratio of line to continuum temperature to derive the electron temperature of the region using equation (2.63). Further, even if one is able to separate out the thermal contribution to the continuum temperature, **it** is still not possible to derive the electron temperature using equation (2.63) with any certainty. This **is** because the thermal continuum is dominated by emission from high density regions ($T_C \propto \int N_e^2 dl$) and as discussed in Chapter 2 the low frequency recombination lines arise mostly in low density regions. Consequently, the line and even the thermal continuum at this frequency arise in

different regions, at least in **the direction** of HII regions. In other directions it is practically impossible to accurately separate the thermal and non-thermal contributions. . Nevertheless the total continuum temperature T_{BC} is an important quantity, to be used in the interpretation of the observed line parameters since it directly affects the line intensity T_L because of stimulated emission.

To derive or put constraints on the properties of the gas responsible for the observed lines it is thus necessary to combine the line parameters observed here with other observations pertaining to the same gas. In the radio frequency range, the low density ionized gas responsible for the lines observed here can manifest itself in the following

1. **Recombination** line emission at different frequencies
2. Continuum emission
3. **Turnover** in the spectrum of non-thermal sources at low frequencies 'if the gas happens to lie along the line of sight.
4. Dispersion of pulsar **signals**

In our interpretation of the line parameters observed here, in terms of the physical properties of the line emitting region, we shall make use of one or more of other available observations when it is reasonable to ascribe them to the same gas. In order that two or more of the observations be useful in putting constraints on a particular parameter of the line emitting region, it is essential that the different observed quantities have very different functional dependences on that parameter. For example, one cannot use recombination lines at two nearby frequencies to put constraints on the density of the emitting region, as the dependence of the line parameters on density will be only marginally different at the two frequencies. In such a case, unless the errors on the observed parameters are infinitesimally small, the uncertainty in the derived parameter will be so large as to make it completely meaningless.

6.2   UPPER LIMIT ON THE ELECTRON DENSITY FROM OBSERVED LINE WIDTHS

As d'iscussed in sections 2.5.I, 2.5.2 and 5.2, the line width due to pressure broadening is directly proportional to the electron density of the region and is a strong function of the principal quantum number $(\Delta\nu_p \propto n^{4.4}$, equation 2.53). This allows us to put an upper limit on the electron density of the regions responsible for the lines from the observed line widths alone.

In figure 6.1 we have plotted the expected width of the H272α recombination line as a function of electron density. The width has been calculated usng equations (2.51), (2.53) and (2.65) for 3 different temperatures and assuming an rms turbulent velocity of $20 kms^{-1}$ which is typical for HII regions. As can be seen from this figure, the width increases sharply for $N_e > 50 \ cm^{-3}$ irrespective of the temperature of the region. 85% of the lines observed in this study have widths < 60 KHz, (see Table 5.2) which corresponds to an upper limit for the electron density of $\sim 60 \ cm^{-3}$. Although the observed widths of the remainder of 15% of the lines are indicated as being > 60 KHz in Table 5.2, they may be made up of multiple components and therefore the actual widths of the individual components can be much smaller. Even so, the maximum width of the line, assuming it to be a single component, corresponds to an upper limit for the electron density of $\sim 100 \ cm^{-3}$. In fig. 6.1, we have also plotted the continuum optical depth at 325 MHz as a function of density assuming a path length of 50 pc. It is interesting that, if these regions have sizes of a few tens of parsecs along the line of sight, then their continuum optical depth at this frequency exceeds unity when the density exceeds $50 \ cm^{-3}$. As discussed in Section 2.5.2, when the region becomes optically thick the recombination lines merge with the .continuum and become undetectable, at least under LTE conditions.

6.3   ANALYSIS OF LINES OBSERVED TOWARDS BLANK REGIONS

Blank regions for our purposes were defined in Section 5.3 as areas in the galactic plane where the continuum emission at
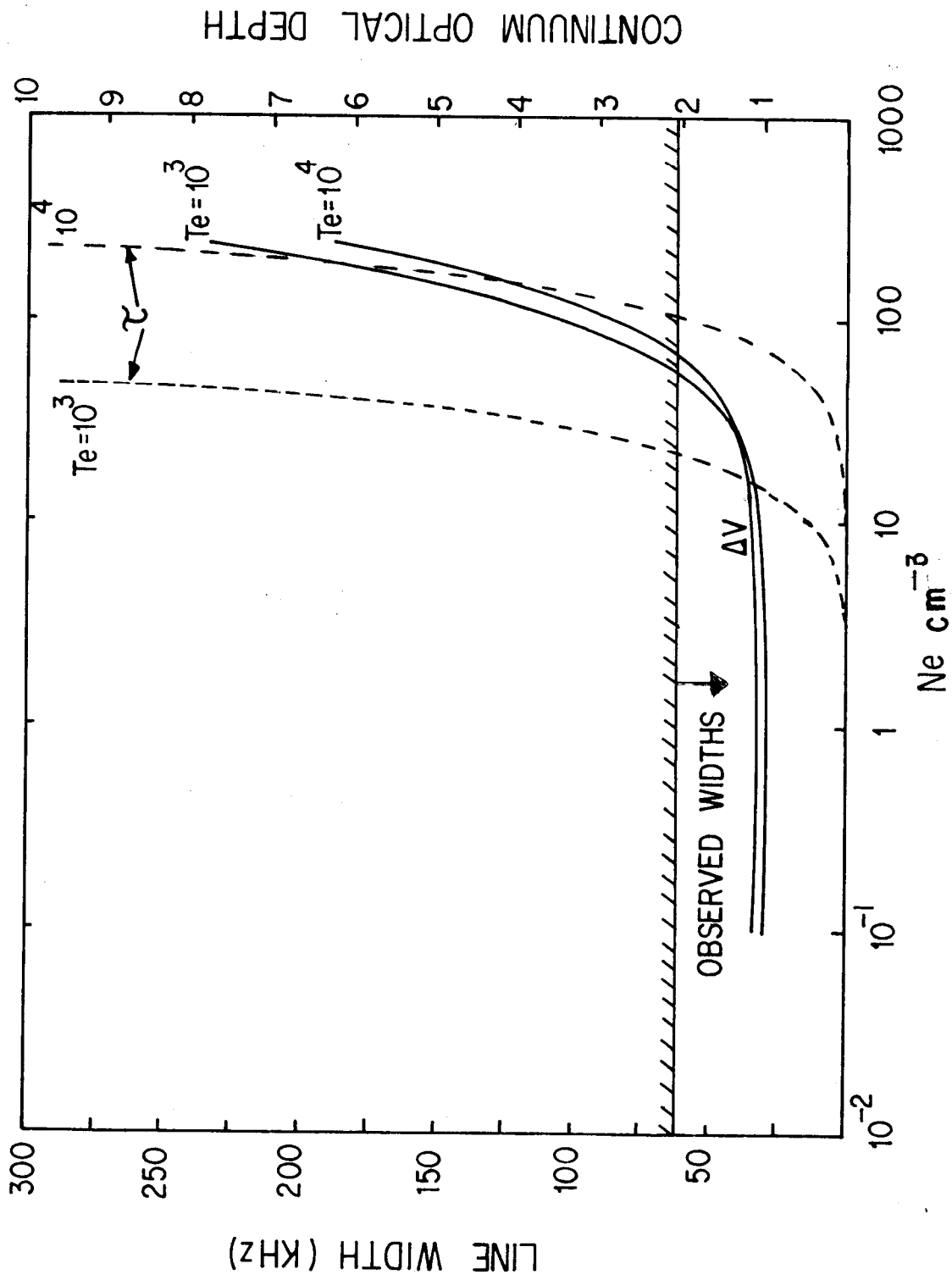
Fig. 6.1 Expected H272α line width (solid curves) as a function of density.
Continuum optical depth at 325 MHz (dashed curves) as a function of
density is also shown. A pathlength of 50 pc is assumed.

5 GHz is a minimum over the telescope beam of 2° x 6' used for these observations. The 5 GHz high resolution map of Altenhoff et al (1978) was used to select 6 such regions. There are no discrete continuum sources within these regions. The positions of these regions are given in Table 5.1. Figure 6.2 shows a typical blank region. The H272α line has been detected towards all the 6 directions and the observed line parameters are given in Table 5.2.

The line emission observed towards blank regions would fall under the category of what is known in the literature as "galactic ridge recombination lines". This refers to the lines observed at higher frequencies towards regions of continuum minimum along the galactic ridge (b = 0). Such lines were first detected near 18 cm (157α line) by Gottesman and Gordon (1970). Subsequently, similar lines have been reported towards selected positions by Gordon and Gottesman (19711, Jackson and Kerr (1971), Gordon and Cato (1972), Gordon et al (1972), Jackson and Kerr (1975) and Mebold et al (1976). The observations of Gordon and co-workers was made near a wavelength of 18 cm corresponding to 157α, Jackson and Kerr near 6 cm corresponding to 110α amd Mebold et al near 11 cm corresponding to 134α. Lockman (1976) and Hart and Pedlar (1976) in another approach have observed the 166α line emission (near 21 cm) at a number of positions along the galactic plane (b=0) separated by 0.5 to 1 in galactic longitude from l=0 to l=70. Some of these positions correspond to regions of continuum minimum as in the case of earlier studies. The general result of all these observations was that the galactic ridge recombination line emission was seen at all longitudes $\lesssim 40^o$. The velocity of the observed lines suggests that the line emitting regions are confined between galactocentric radii of 4 and 8 kpc.

The observation towards blank regions in the present study is the first complementary information available at a lower frequency for understanding the properties of these line emitting regions. In this section we shall make use of the line parameters observed here and at higher frequencies mentioned
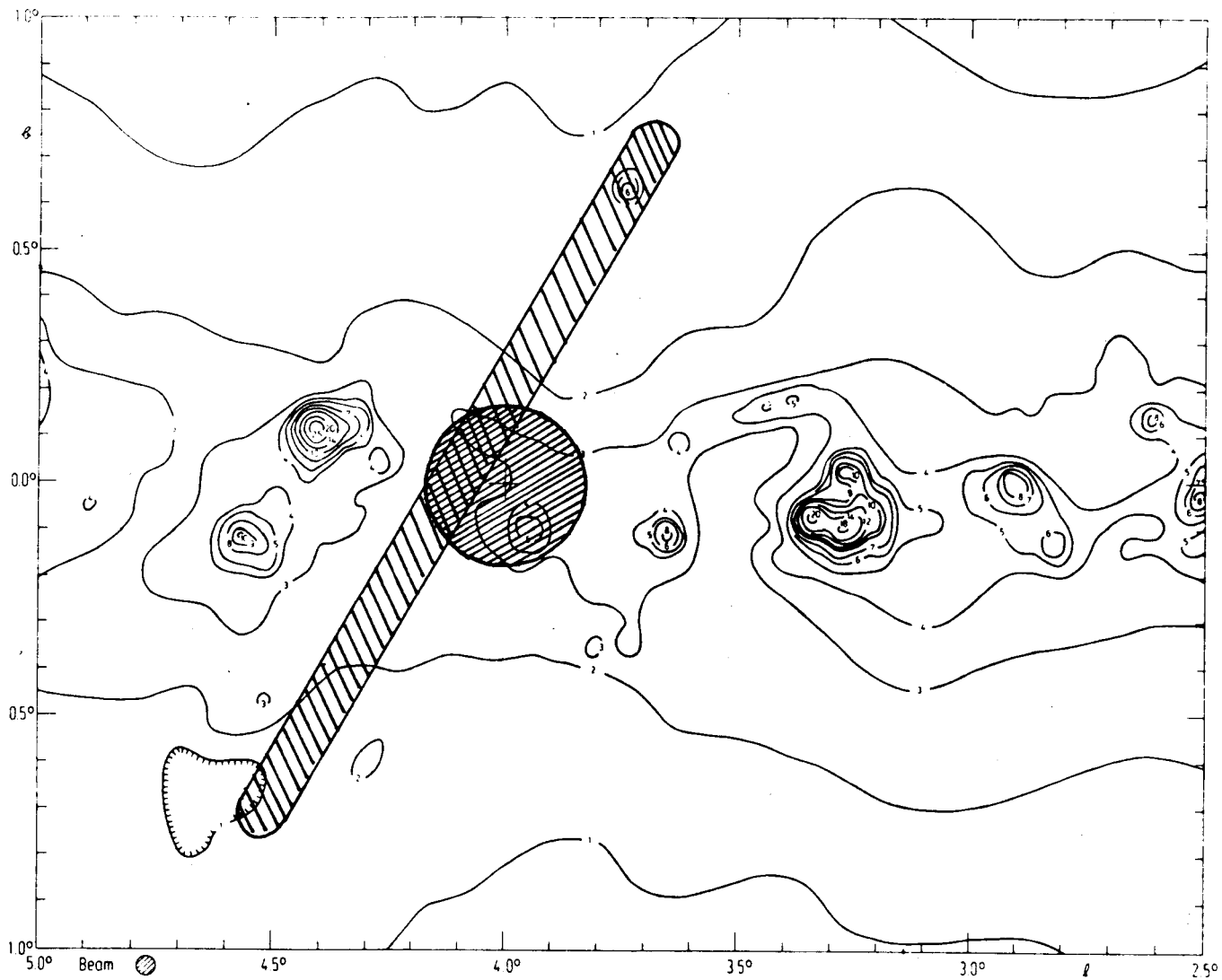
Fig. 6.2   A typical blank region (G4.2-0.0).   The elongated hatched area represents the ORT beam.   The circle indicates the nearest 166   position observed by Lockman (1976).   The' 5 GHz continuum map is from Altenhoff et.al. (1978).

above to determine or put constraints on the parameters of the line emitting region. As stated earlier, we can only determine those parameters which have very different functional dependences on the observable quantities like line temperature' T_L and width Δv.

The observed width ΔV can be used to set an upper limit on the electron density N_e of the region as discussed in Section 6.2. In principle ΔV can also be used to set an upper limit on the electron temperature T_e of the region assuming that all of the observed width arises due to thermal motions. But for $\Delta v > 25 \text{ kms}^{-1}$, which is the case for most of the observed lines, the effective doppler temperature (equation 2.5.1) exceeds 27000K and therefore it is not a meaningful limit. We shall now investigate the dependence of the line intensity T_L as a function of N_e and T_e at two frequencies corresponding to 166α and 2724. To be able to do this we first need to have the departure coefficients b_n and their derivatives β_n (see Section 2.6.1 and 2.6.4) as a function of N_e and T_e and for the required levels.

6.3.1   Calculation of the Departure Coefficients:

The most recently published table of departure coefficients for hydrogenic atoms is that of Salem and Brocklehurst (1979). The tabulated values are for a range of electron density (of HII regions) from 10 to 10^5 cm^{-3} and electron temperature from 10 to $10^{4.5}$ K, with no background radiation. The departure coefficients for $N_e < 10$ cm^{-3} and $T_e < 10^3 k$ are not available in this table and the published values do not take into account the effect of external radiation. We therefore obtained a copy of the computer program published by Brocklehurst and Salem (1977) and used it on a PRIME 450 computer to calculate the departure coefficients for the required ranges of N_e and T_e , taking into account the effect of the galactic non-thermal background.

The b_n and β_n values were calculated for 12 temperatures in the range 25K to 10000K and 14 electron densities in the range

0.005 cm to 100 cm^{-3}. A radiation field characterized at any frequency by

$$T_{R\nu} = T_{R408} \left(\frac{\nu_{MHz}}{408} \right)^{-2.7} \tag{6.1}$$

was used in the calculation. An average value of $T_{R408} = 400K$ representing the galactic non-thermal background was estimated from the 408 MHz continuum maps of Haslam et al (1982). Since this radiation is present everywhere within the galaxy, a dilution factor of unity was used.

For each combination of N_e and T_e (there are 14x12=168 such combinations) the program was used to calculate the departure coefficients b_n and their derivative β_n for n = 50 to n = 507. The calculated values for all the n's and all the combinations of N_e and T_e were made into a data file from which a simple interpolation program extracts b_n and β_n for a specified N_e, T_e and n. In all the calculations that follow, these values of b_n and β_n will be used.

6.3.2 Intensity of 166α and 272α lines as function of N_e and T_e

An expression for the excess temperature observable by a radio telescope at the recombination line frequency is given by equation 2.77 as

$$T_L = T_0 \left(e^{-\tau_c} (e^{-\tau_L} - 1) \right) + T_e \left[\frac{b_m \tau_L^* + \tau_c}{\tau_L + \tau_c} (1 - e^{-\tau_c + \tau_L}) - (1 - e^{-\tau_c}) \right]$$

$$+ T_N \left[\frac{1 - e^{-(\tau_L + \tau_c)}}{\tau_L + \tau_c} - \frac{1 - e^{-\tau_c}}{\tau_L} \right] \tag{2.77}$$
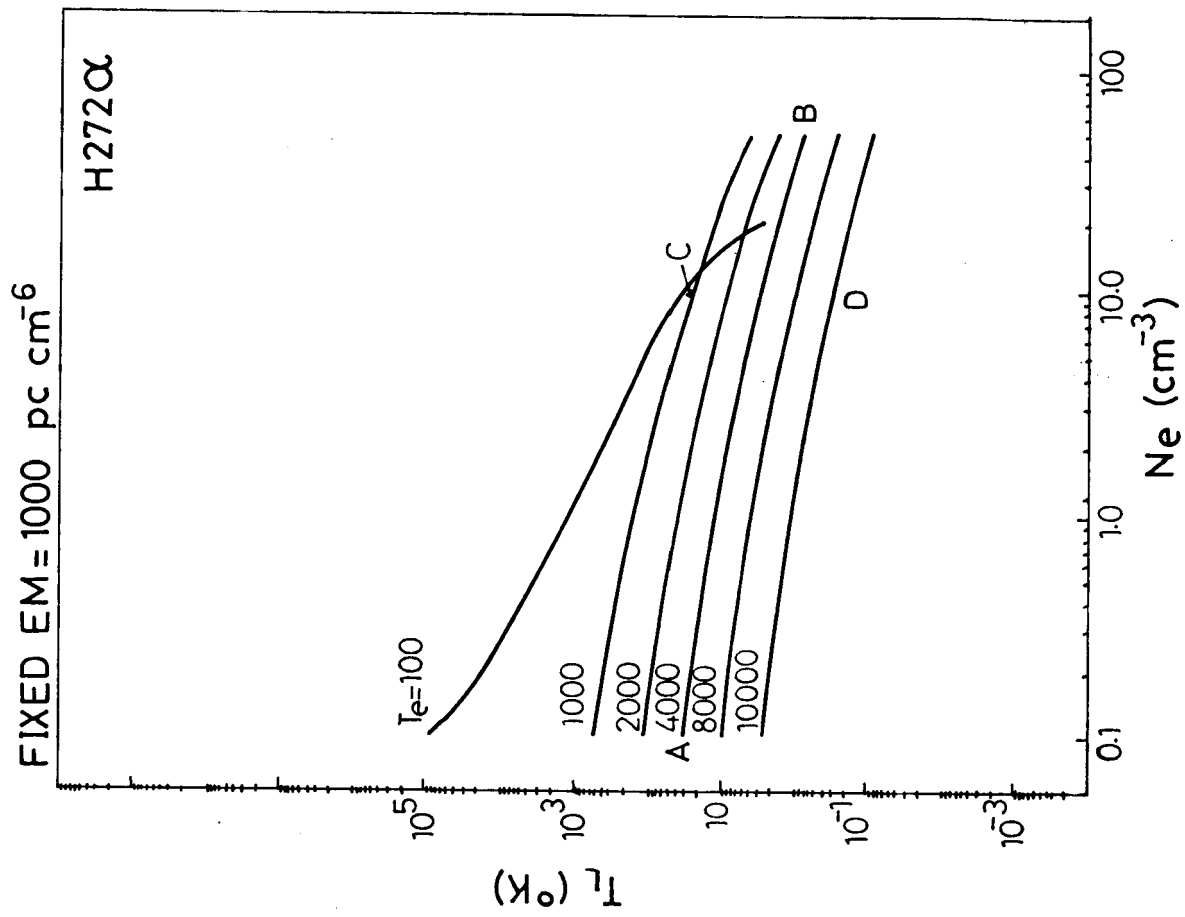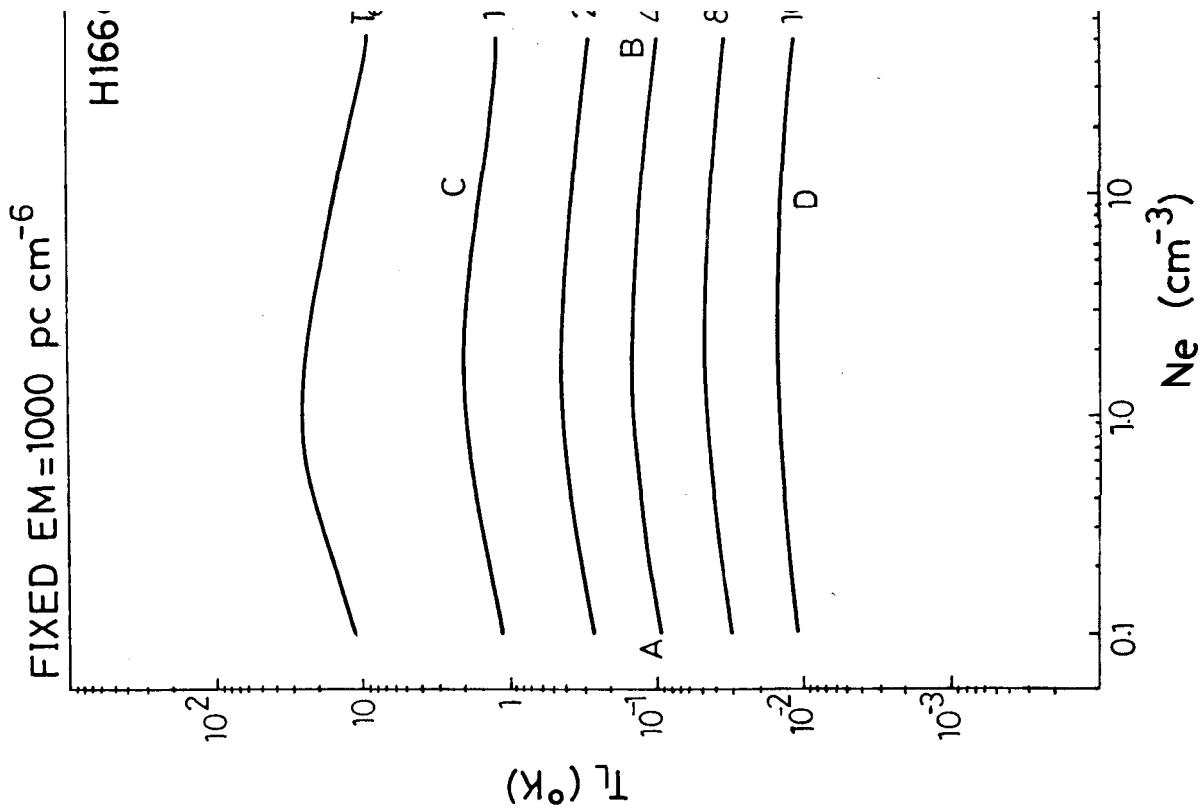
where T_0 = Continuum temperature of the background source

T_e = Electron temperature of the gas

T_N = The non-thermal background distributed inside the cloud

τ_L^* = LTE optical depth given by eqn. 2.48

$\tau_L = b_n \beta_n \tau_L^*$ the true optical depth

τ_c = Continuum optical depth given by eqn. 2.11

To calculate the line intensity we have used a simple plane-parallel model of uniform density and temperature. The cloud and the background source were assumed to fill the telescope beam The line of sight was considered to be free of any discrete continuum source. We further assume that the cloud is situated half way to the edge of the galaxy along the line of sight so that we can write $T_0 = T_{Bg}/2$ where T_{Bg} represents the galactic non-thermal radiation. We have used equation 6.1 to calculate the T_{Bg} (with $T_{B408} = 400K$) at the line frequency. T_N was set equal to zero. We have used $\Delta V = 50$ kms^{-1} which represents the typical width of the galactic ridge recombination lines.

In Figure (6.3) we have plotted the calculated 1669 line temperature as a function of electron density for different electron temperatures and a fixed emission measure = 1000 cm^{-6} pc. Figure (6.4) is a similar plot for the calculated 272α line temperature. Figure 6.3 shows that for a given temperature the intensity of the 166α line is practically independent of density provided the emission measure is fixed. For example a change in density of 3 orders of magnitude (going from point A to point B) hardly changes the line temperature by a factor of 2. Whereas a **similar change in density causes the intensity of tho 272α line** (point A to B in fig. 6.3) to change by a factor of more than 35. Thus the line intensity is a very different function of electron density in the two cases. Therefore if one observes 166α and 272α line from the same region, it will be possible to put strong constraints on the electron density of the medium On the other hand, the intensities of the two lines vary very similarly with electron temperature. In figure (6.3) and (6.4) the intensities of both the lines change by a factor of ~150 when the temperature is varied from 1000 to 10000K (going from point C to D).

When the path length through the gas is fixed, the intensity of the two lines is again found to vary very differently as a function of density. In fig. (6.5) the 166α line intensity is seen to change by 6 orders of magnitude in going from point A to

FIXED EM=1000 pc cm^{-6}

H272α

T_e=100

1000

2000

A 4000

8000

10000

C

B

D

T_L (°K)

N_e (cm^{-3})

0.1   1.0   10.0   100

FIXED EM=1000 pc cm^{-6}

H166

C

A

B

D

T_L (°K)

N_e (cm^{-3})

0.1   1.0   10 10^2

Figs. 6.3   Expected peak line temperature of H166α and H272α lines as a function of
and 6.4   density for different temperatures. EM is fixed at 1000 pc cm^{-6}.
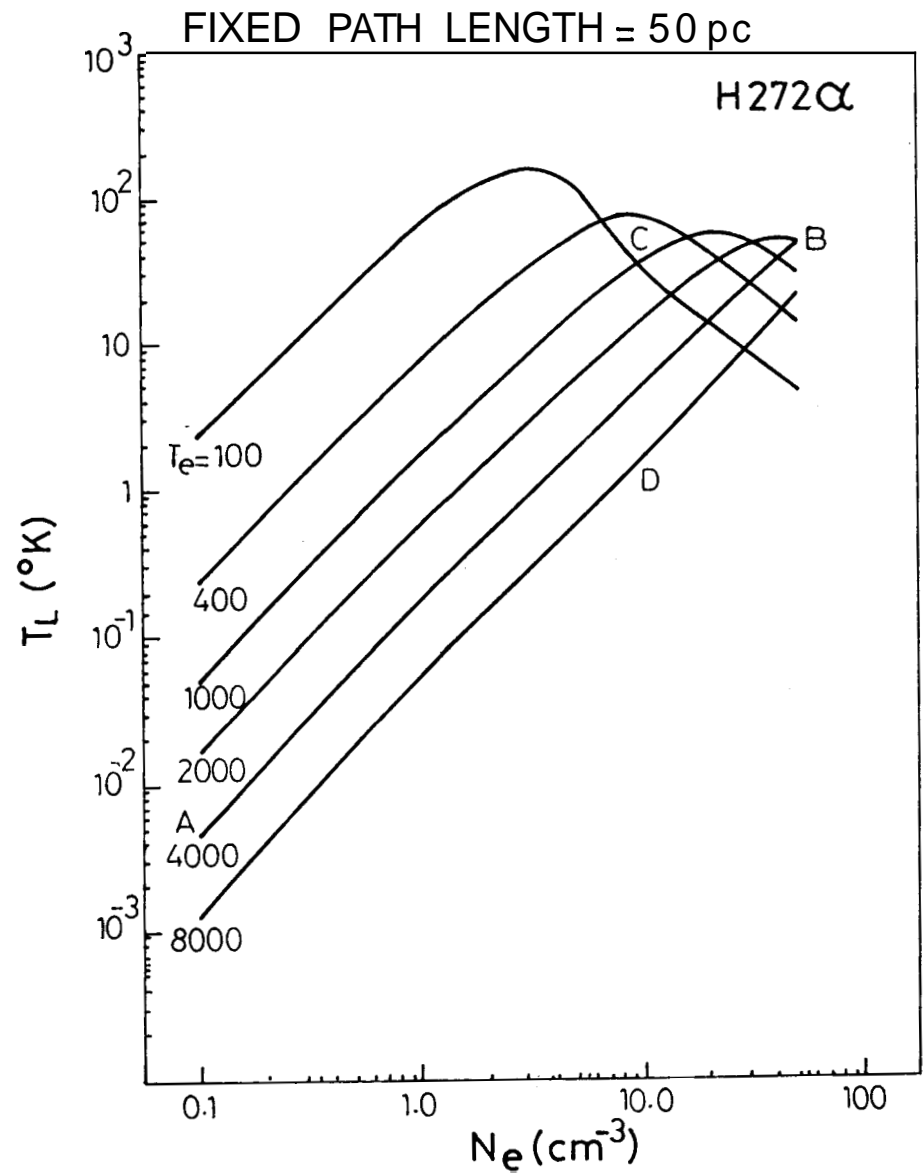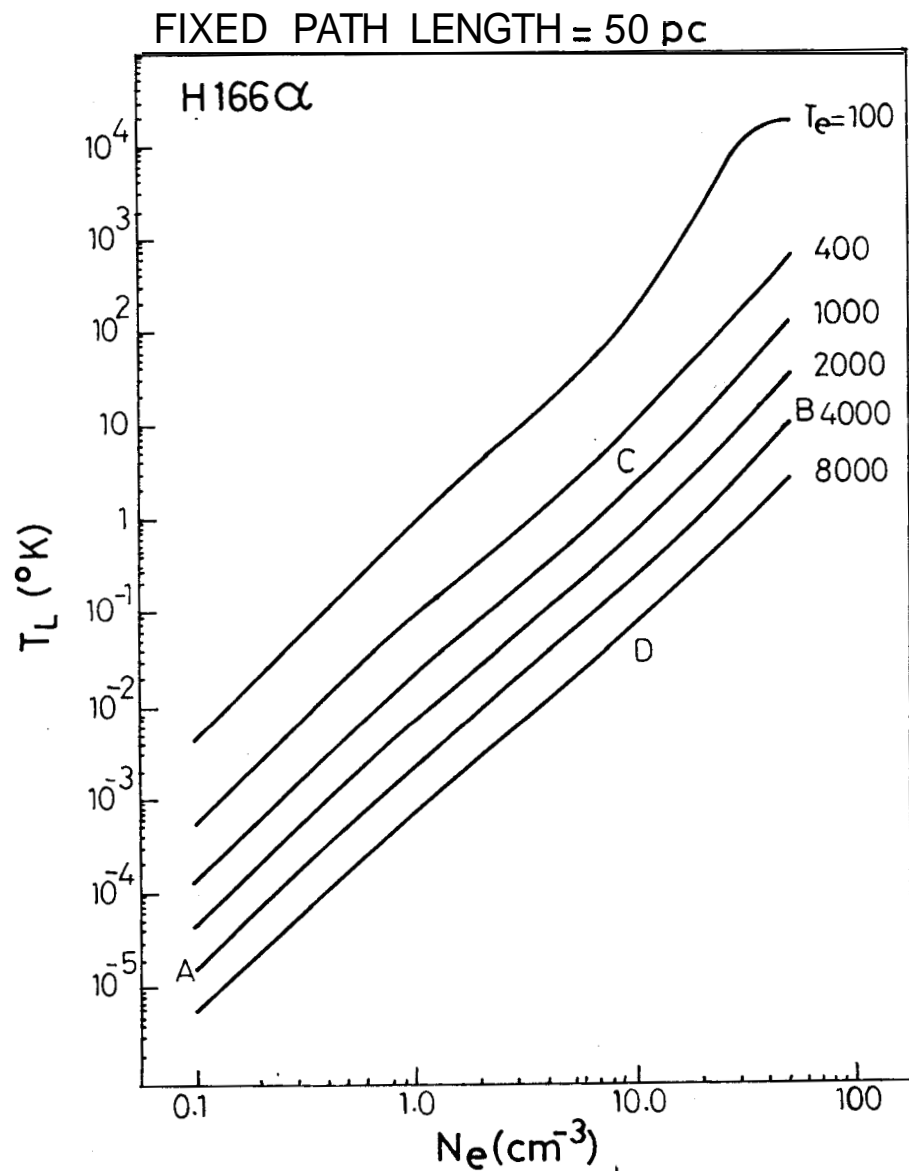
Figs. 6.5 and 6.6   Expected peak line temperature of H166α and H272α lines as a function of N_e for different temperatures. The effective pathlength is fixed at 50 pc.

B whereas the 272α line intensity (fig. 6.6) changes by 3 orders of magnitude. In other words the intensity of the 166 line varies nearly as the emission measure of the region (square of the electron density for fixed pathlength) and that of the 272α line almost as the density of the region. As a function of temperature the corresponding changes for 166α and 272α lines (in going from C to D in figs. 6.5 and 6.6) are about 25 and 15 respectively. Therefore for a fixed path length the difference in the dependence of the two line intensities as a function of temperature is less than a factor of 2. It appears that some other observed quantity has to be used to put constraints on the electron temperature.

The drastic difference between the dependences of the two line intensities on density (for both fixed EM and fixed path length) is a consequence of the dominance of the spontaneous line emission in the case of 166α, and that of stimulated emission by the background radiation in the case of 272α. The contribution to the line intensity due to stimulated emission by background radiation is given by the first term of equation 2.77 namely

$$T_0 \left[e^{-\tau_c} \left(e^{-\tau_L} - 1 \right) \right]$$

and the line optical depth τ_L is given by

$$\tau_L = b_n \beta_n \tau_L^*$$

where τ_L^* is the LTE optical depth and β_n is related to the derivative of the departure coefficient b_n. The value of $1 - \beta_n$ describes the relative population of the adjacent levels. In fig. 6.7 we have plotted $1 - \beta_n$ for n = 166 and n = 272 as a function of density for a temperature of 5000K. As can be seen in this figure β_{272} changes by a factor of about 50 over the density range considered in the above calculation of line intensities, whereas β_{166} changes only by a factor of 6. In addition, the background radiation T_0 which has a non-thermal spectrum, is about 360K at the frequency of 272α while at that of 1664 it is 6K. This difference in the strength of the radiation coupled with the large difference in the rate of variation of
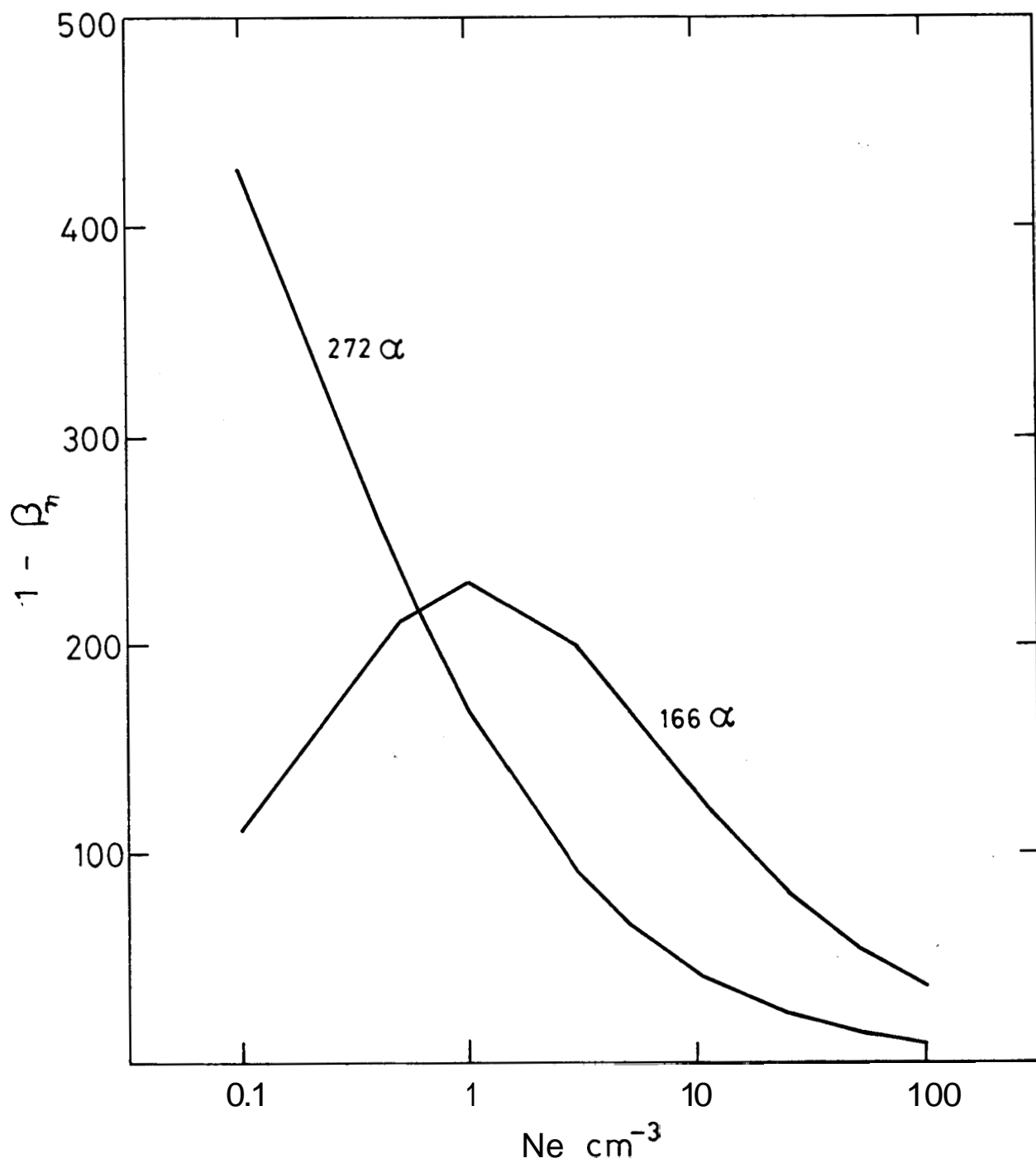
Fig. 6.7   The derivative of the departure coefficients $(1-\beta_n)$
as a function of N_e for n = 272 and n = 166.

β_m with density, makes the line intensity at the two frequencies have very different dependences on the electron density.

6.3.3 A Model for Interpretation of the Observed Line Intensities

We shall adopt a simple plane parallel homogeneous cloud model in which the electron temperature T_e and the electron density N_e are uniform   The. model is illustrated in fig. 6.8. The cloud extends over a path length L along the line of sight, resulting in an emission measure EM = $N_e^2 L$. T_0 represents the radiation originating behind the cloud. As we are considering blank regions most of the observed continuum temperature T_{BC} is due to the galactic background. Since we do not know the precise location of the cloud along the line of sight (the observed line velocity has a distance ambiguity), we assume that half of the observed T_{BC} originates behind the cloud. It is reasonable to assume that the background radiation is uniform over the telescope beam Ω_B , but the cloud cannot be assumed to fill the telescope beam of 2° x 6' used for the 272α observations. We estimate a beam dilution factor as follows. Hart and Peldar (1976) have found that the 166α line emission at b = $\pm 0^{\circ}.5$ (l=25°) falls to less than 50% of the intensity at b=0°. Lockman (1976) also finds that the 166α line intensity falls to 50% at b = $\pm 0^{\circ}.5$ (for l = 26$^{\circ}.5$) compared to the emission at b = 0° . Gottesman, Brown and Gordon (1972) from their observation of the 1574 line also conclude that the line emission is confined to b = $\pm 0^{\circ}.5$. The 2° east-west beam of the Ooty telescope extends to b = $\pm 0^{\circ}.8 - 0^{\circ}.9$ when pointed at b = 0° over the longitude range observed here.   Taking the average extent of the gas in latitude to be $\sim \pm 0^{\circ}.5$ we get a beam dilution factor of $0.5/0.85 = 0.6$.   In all our analysis we have used this value for beam dilution, for the 272α line.

In this model the expected line brightness temperature T_{BL} is given by

$$T_{BL} = \frac{\Omega_C}{\Omega_B} \times T_L \qquad\qquad (6.2)$$

where (Ω_C / Ω_B) is the beam dilution factor, and T_L is the line

Back ground source

CLOUD

Telescope.

o

Beam size
Ω_B

Observed quantities.
$T_{BL}, \Delta V, T_{BC}$

o

Background Radiation $T_\emptyset$

Electron temp Te
Electron density Ne.
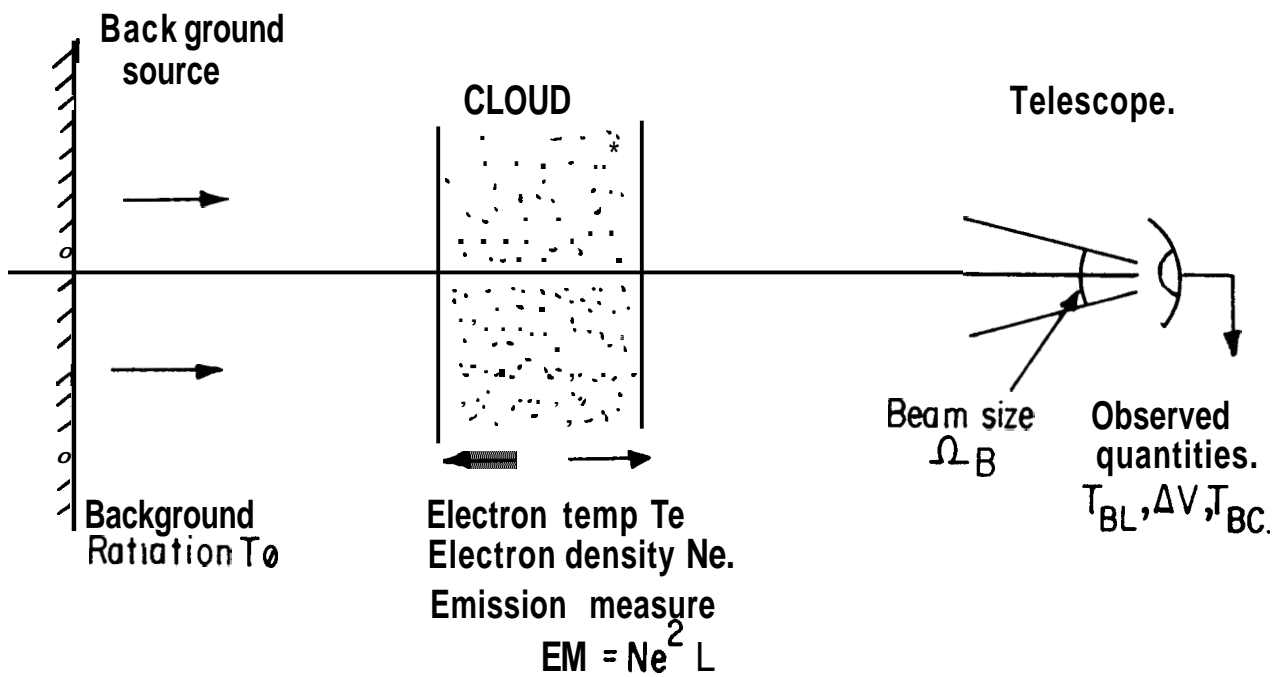**Emission measure**
$$EM = Ne^2 L$$

FIG.6.8. A MODEL FOR GEOMETRY OF BACKGROUND
SOURCE AND THE LINE EMITTING CLOUD.

temperature calculated using equation (2.77). For any specified value of Ne, Te, EM and line width ΔV the line and continuum optical depths τ_L and τ_c can be calculated using equations (2.71), (2.481, (2.571, (2.54) and (2.13). b_n and β_n can be obtained as described in Section 6.3.1. Further, if T_0 and T_N are given, the expected T_L can be calculated using equation (2.77).

6.3.4 Electron Density of the Gas

From the discussion in Section 6.3.2 it is clear that strong constraints can be imposed on the electron density of the line emitting region if both 166α and 272α lines are observed from the same gas. If we use the above model it turns out that the electron density gets almost uniquely determined if we use the observed intensities of the 166α and 272α lines.

We shall make use of the 272α line parameters observed here together with those of the 166α line observed at nearby positions by Lockman (1976) to derive the electron density of the gas responsible for the line emission. The 166α line measurements are available within 0f3 in longitude for all the blank regions observed here and for two of the positions the 166α measurements are within the Ooty beam. The observed 272α line parameters, T_{BL}, ΔV and V_{LSR} and the measured total continuum temperature T_{BC} are given in Table 6.1 for all the blank regions. The peak 166α line temperture observed by Lockman (1976) at the nearest position is also given in this table. Lockman (1976) has not given the width of the line, and we will therefore use the observed width at 272α for calculating the expected line temperature at the two frequencies. We assume that the two observations pertain to the same gas.

Using equation (2.77) and model described above, it is possible to find those combinations of Ne, Te and EM which produce the observed intensities of both the 166α and the 272α lines. The procedure adopted was as follows.

TABLE 6.1 : Observed Parameters for Blank Regions

	H272α Parameters				H166α [1]		5 GHz continuum Temp[2]
G number	Line Temp °K	Width ΔV km/s	V_{LSR} km/s	T_{BC} (°K)	T_L (°K)	T_C (°K)	°K
G2.1-0.0	0.81(0.13)	47(4)	5(2)	740	<0.016	13.3(1.2)	0.56
G4.2-0.0	1.28(0.24)	33(5)	7(2)	690	0.045(15)	10.0(0.5)	0.4
G9.4+0.1	0.61(0.13)	42(7)	10(3)	730	0.054(14)	12.1(0.7)	0.4
G15.7-0.0	0.86(0.14)	58(5)	43(2)	610	0.051(15)	8.9(1.0)	0.36
G17.6-0.3	0.67(0.11)	47(4)	30(2)	630	0.027(14)	8.1(1.2)	0.34
G21.2-0.0	0.64(0.11)	26(3)	98(2)	580	0.038(15)	10.4(0.7)	0.34
	0.46(0.08)	54(6)	25(3)				

1. From Lockman(1976)
2. Estimated from the maps of Altenhoff et al (1978)

For a set of specified N_e and   , in the range 0.1-100 cm^{-3} and 100-10000K respectively, the emission measure required to produce the observed intensity of the 272α line was calculated using equation (6.2) and (2.77). An iterative procedure was used to arrive at the required emission measure. The background temperature T_0 in equation (2.77) was taken to be $T_{Bc}/2$ (Table 6.1). As the path lengths involved are not very large, we used T_N =0. A dilution factor (Ω_c/Ω_B) = 0.6 was used in all the calculations. Similarly, calculations were performed to obtain the required emission measure to produce the observed 166α line intensity given in Table 6.1 for the same direction. As the beam size used for the 166α line was 21 arcmin, we used a dilution factor of unity. We again used $T_0 = T_B/2$ and T_N = 0. For both 166α and 272α lines the width ΔV observed at 272α was used for the calculations.

The results of these calculations are shown in figures 6.9 and 6.10 for two blank region positions G4.2-0.0 and G9.4+0.1. In these figures we have plotted the required emission measure as a function of electron density N_e to produce the observed intensities of the 272α and 166α lines, for 4 different electron temperatures. The intersection point of the 272α and 166α curves at each of the temperatures gives the electron density N_e (and the corresponding EM) which will explain both the observed 166α and 272α line intensities. It is remarkable that irrespective of the temperature T_e and emission measure EM of the region there is only a very small range of electron densities (bounded by the two vertical dashed lines) that is permissble in order to account for both the line intensities. This range is less than a factor of 1.5 and for temperatures above 1000K the required density has practically a unique value.

The accuracy of the electron density determined in this fashion depends only on the accuracy of the measurements of the line parameters and that of the estimated beam dilution factor. When the errors on the line intensities are taken into account the derived density is within a factor of 2. If the beam dilution changes by a certain factor then the derived density
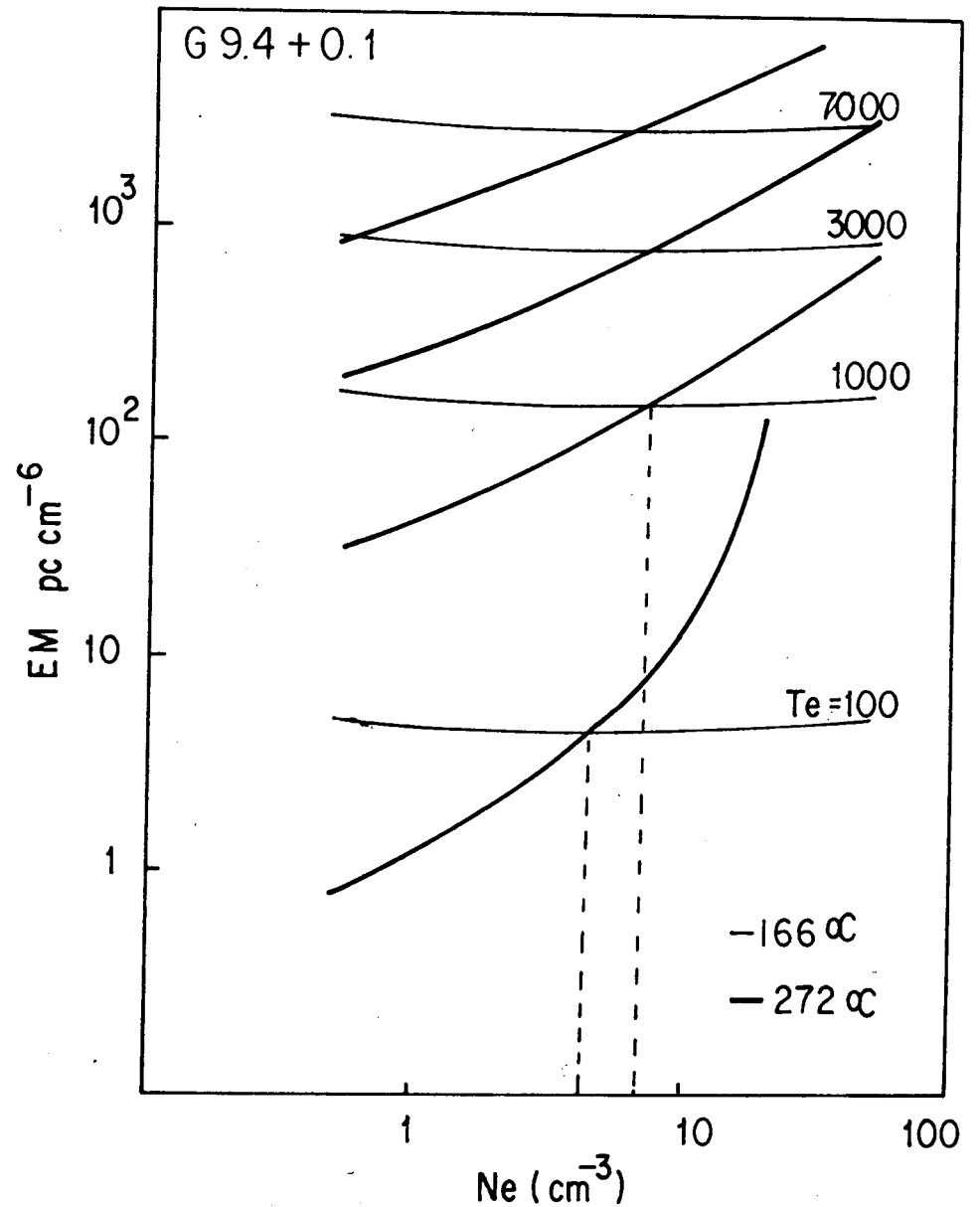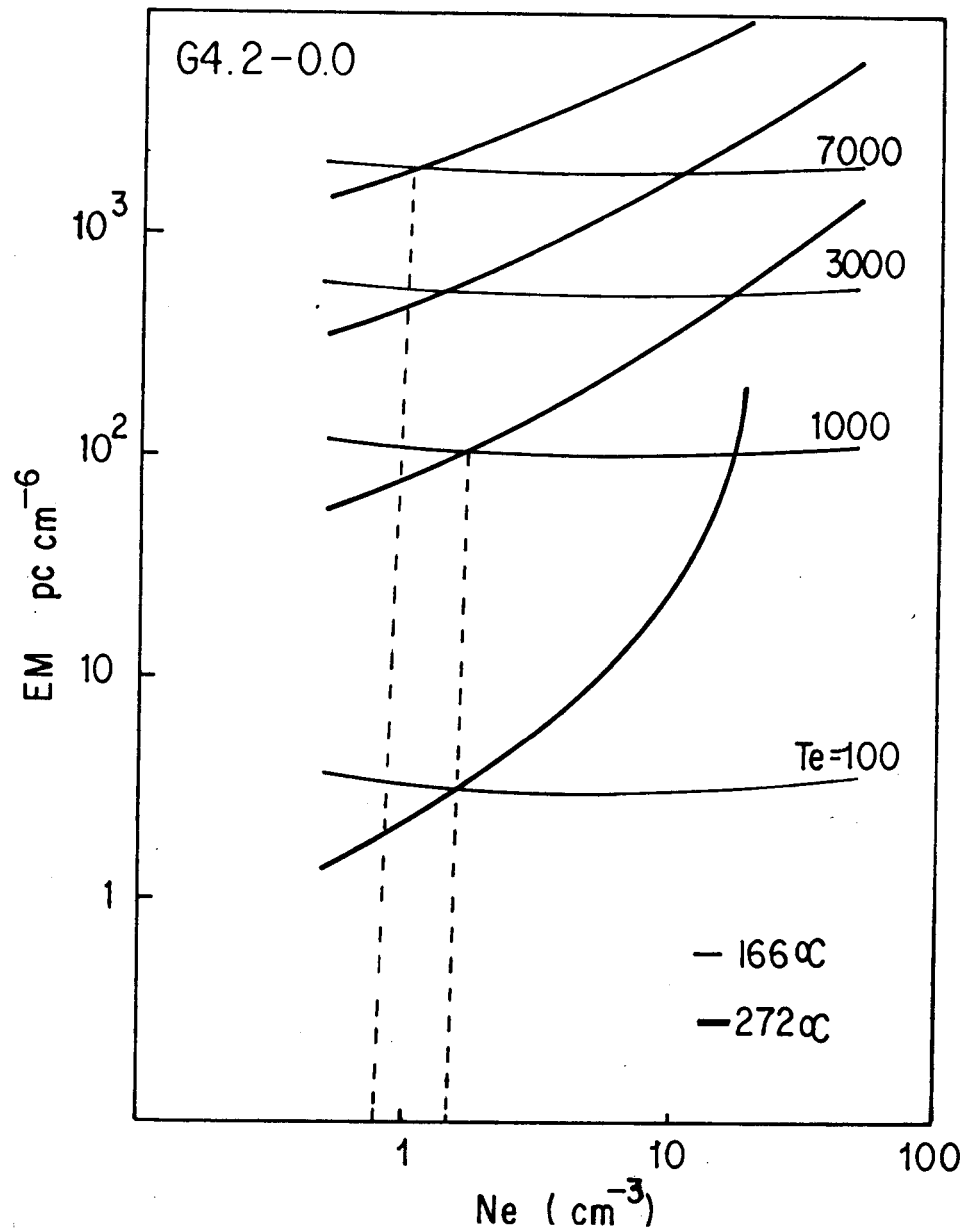
Fig. 6.9 and 6.10   Emission measure as a function of Ne, required to produce the observed H272α and H166α lines at different temperatures. The intersection of thick and thin lines give the density of the gas.

changes by a similar factor. An increase in the beam dilution (i.e. smaller angular size for the cloud) for the 2724 line results in a decrease in density. Increase in T_0 also increases the derived density.

The densities derived from similar calculations for all the blank regions is given in column 2 of Table 6.2. They are in the range of 0.5-6 cm^{-3}. These densities are reliable to' within a factor of 2. It should be noted here that these densities are the true electron densities of the line emitting regions and not the average electron density as in the case when it is derived (for strong HII regions) from continuum measurements. In the latter case, as also in the case of high frequency recombination lines, the emission is proportional to the square of the electron density. But at low frequencies, due to the strong dependence of b_n and particularly β_n on the electron density, the strength of the line emission is proportional to the density itself. Therefore, if there is any clumping in the gas, then the clumps themselves should have this derived density and the size of the region should increase to make up for the decreased filling factor. In other words, if the emission measure of this gas is fixed, say by other considerations, then the size of the region (along the line of sight) can be $\geqslant EM/N_e^2$ depending on the filling factor of the ionized gas at density N_e .

It is worth noting here that high frequency recombination line measurements alone cannot be used to derive the electron density of a medium as the line intensity at these frequencies depends only on the EM due to the dominance of spontaneous emission. This is seen even in the case of the 166α line (1420 MHz) in fig. 6.9 and 6.10 in which a nearly constant EM is required to produce a given line intensity irrespective of the density. A non-LTE analysis of a high frequency line like 109α can only lead to the determination of the electron temperature. On the other hand, as demonstrated here, a low frequency recombination line measurement (like the 272α) can lead to a determination of the density.

TABLE 6.2 :Derived Parameters For Blank Regions

| G number	N_e cm^{-3}	Upper limits from T_c(5GHz)			Upper limits from PSR DM			Lower limits with L >50pc	
		EM cm^{-6}pc	T ^{c}K	L PC	L pc	EM cm^{-6}pc	T ^{c}K	EM cm^{-6}pc	T ^{c}K
G2.1-0.0	0.5	4000	11000	16000	800	200	2100	12.5	500
G4.2-0.0	1.0	3600	10000	3600	400	400	2500	50	800
G9.4+0.1	6.0	3500	8000	97	60	2160	6000	1800	5000
G15.7-0.0	2.5	2800	5000	448	160	1000	3100	312	1300
G17.6-0.3	2.0	2500	7000	625	200	800	4000	200	1600
G21.2-0.0	4.0	2500	8500	156	100	1600	6000	800	4000

6. 3. 5   Electron temperature and Emission measure:

Having derived the electron density of the gas responsible for the observed lines in the blank regions, we can now turn to the two other parameters T_e and EM which charaterize the line emitting region. Since in the model we are considering there are only 3 parameters N_e, T_e and EM which characterize the ionized region, and we have used 2 measured quantities (the intensity of the 166α and 272α lines) to determine one of these, namely N_e, the other two parameters T_e and EM get related to each other through the observed intensity of the 166α or the 272α line. The method used for determining the electron density ensures that the relation between T_e and EM will be very similar irrespective of whether we use the 1664 or the 272α line intensity to relate them. A determination of, or putting a constraint on, either T_e or EM (or even the path length L) will decide or impose a constraint on the other quantity.

Figures 6. 11 and 6. 12 show the relation between EM and T_e in order that the region produces both the observed 272α and 166α intensities. The lines marked 2724 and 166α in these figures represent EM as a function of T_e required by the intensity of these lines, given that the electron density N_e of the region is as obtained in the previous section. As expected, the two curves are very similar. On the ordinate is also marked the effective path length obtained simply from the relation L = EM/ N_e^2 .

Unfortunately, there is no other measured quantity available which can be directly attributed to this gas and which depends on T_e , EM or L in a different way, to impose a constraint on any of these parameters. However, we can put some **limits** on these parameters from **3** considerations.

The first of these is based on the thermal continuum emission from this gas. At a sufficiently high frequency like 5 **GHz,** the contribution to the galactic background from the non-thermal radiation is very small particularly in the blank
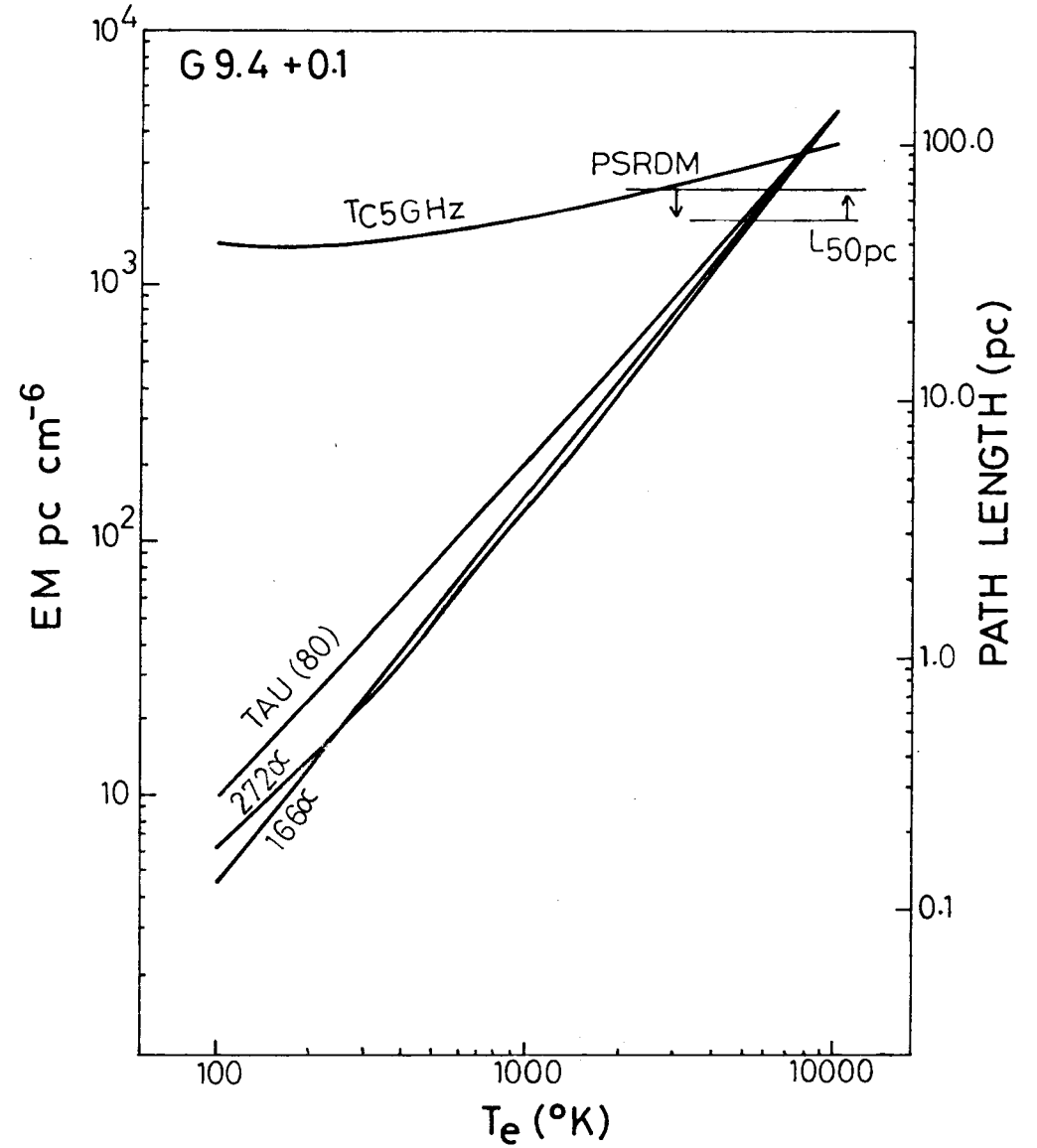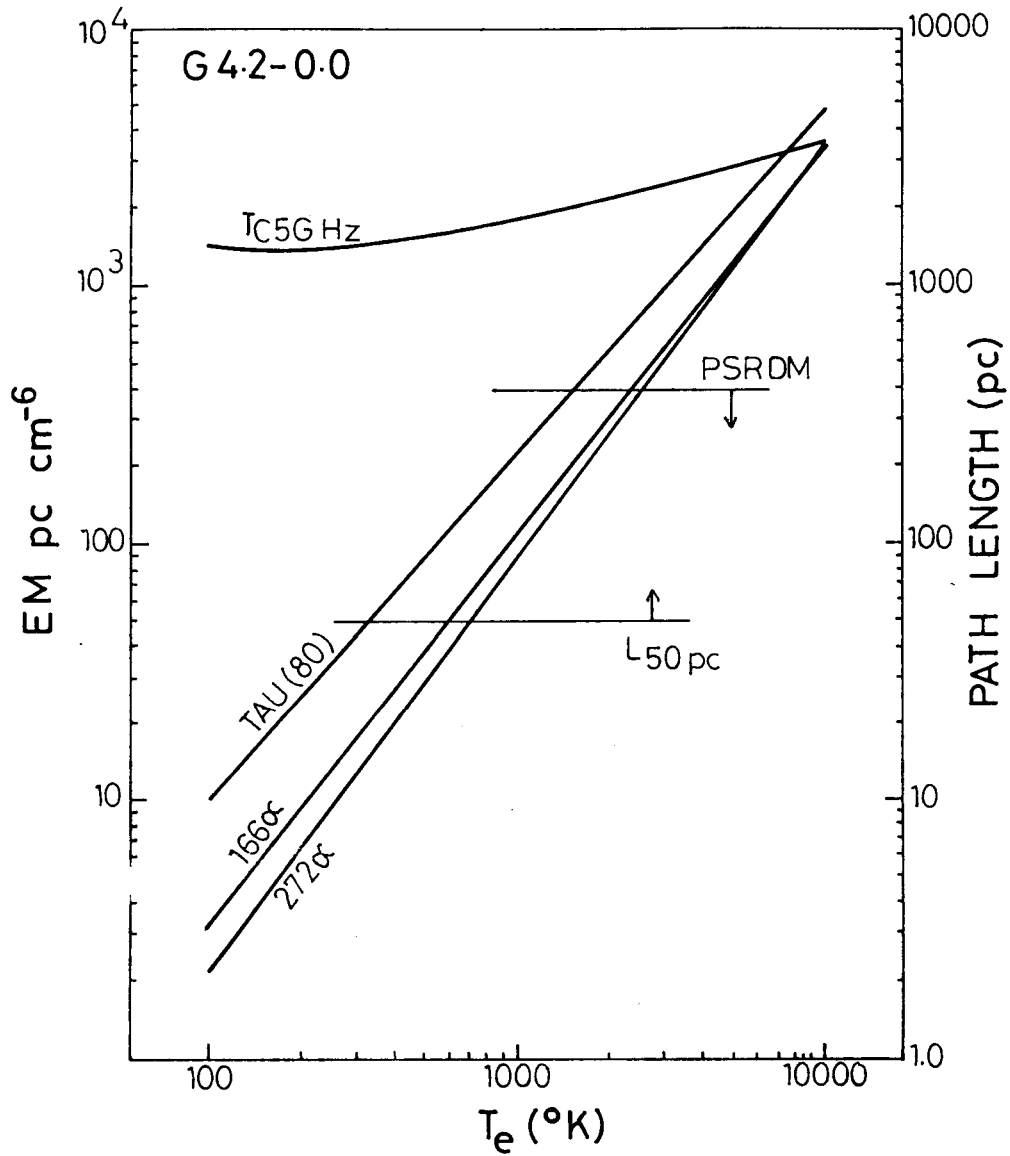
Figs. 6.11 and 6.12   Relationship between EM and T_e to produce the observed 272α and 166α line intensities, towards two blank regions. N_e is determined from figs. 6.9 and 6.10. The limits implied by T_c (5GHz), pulsar DM and pathlength are also shown (see text).

areas. Therefore most of the observed continuum at 5 GHz will be thermal. We have estimated the average continuum temperature at 5 GHz at each of the observed blank regions using the high resolution maps of Altenhoff et al (1978). The estimated values are given in Table 6.1 for all the blank regions.

We cannot demand that all of this observed continuum temperature be produced by the ionized regions responsible for the recombination lines. This is because there will still be some non-thermal contribution at this frequency and in addition there may be other gas along the line of sight which can contribute to the observed continuum But we can certainly require that the ionized gas which produces the recombination lines should not produce more than this observed continuum This will impose an upper limit on the EM of the gas which in turn will imply an upper limit on the electron temperature through the already established relation between them The expected continuum brightness temperature can be calculated given T_e and EM using equations (2.14) and (2.13). The nearly horizontal line marked TC5GHz in figures 6.11 and 6.12 represents the constraint on the EM of the gas based on the 5 GHz continuum temperture listed in Table 6.1. The emission measure cannot be above this line. Combining this limit with the relation between EM and T_e we can get an upper limit for T_e. The upper limits obtained this way for all the blank regions is given in Table 6.2. The upper limits for EM are in the range of 2500-4000 cm^{-6} pc and for T_e in the range of 5000-10000K.

Given the density of the gas an upper limit on its path length can be imposed using the pulsar dispersion measure. The presence of ionized gas along the line of sight to a pulsar causes dispersion of the signals received from it. By measuring the time delay in the arrival of the pulses at different frequencies one can obtain what is called the dispersion measure (DM) which is defined as $DM = \int_0^d N_e^2 \, dL$ where d is the distance to the pulsar. Vivekanand and Narayan (1982) have analysed the DM towards 224 pulsars and have obtained a model for the galactic electron density of the form

$$N_e(z) = 0.030 + 0.020 \, exp\left(-\frac{|z|}{70}\right) \, cm^{-3} \quad (6.3)$$

where Z (pc) is the height above the galactic plane. The first term in this expression represents a distibuted medium of average $\langle Ne \rangle = 0.03\,cm^{-3}$ having a scale height in excess of 300 pc. The second term describes the contribution from localized higher density ionized regions (e.g. HII regions) which occur in the galactic plane with a scale height of 70 pc. The regions responsible for the recombination lines observed towards blank regions can be considered to fall in this category.

The meaning of the second term in equation (6.3) is that in the galactic plane at $b = 0^{\circ}$ the electron density along any line of sight, averaged over the entire path length through the galaxy (which may intersect some HII region) is $0.02\ cm^{-3}$. We can use this result together with Ne determined for the blank regions to set an upper limit to the effective path length through the gas responsible for the recombination lines.

If Ne is the density of a region lying along a line of sight and L_{gal} is the path length through the entire galaxy then the above result imposes a restriction on the effective path length L through the region of the form

$$Ne \cdot \frac{L}{L_{gal}} \leq 0.02\ cm^{-3}$$

$$\text{or} \qquad L \leq \frac{0.02}{Ne}\ cm^{-3}$$

using the Ne determined for the blank regions and taking $L_{gal} \gtrsim 20$ kpc we obtain upper limits of 60-400pc for the effective path length through the gas responsible for the observed lines. The horizontal lines marked PSRDM in figures 6.11 and 6.12 represent these upper limits, for the blank regions G4.2-0.0 and G9.4+0.1. The upper limit on L implies an upper limit on EM which in turn implies an upper limit on Te. These upper limits are also given in Table 6.2. In most of the cases these upper limits are lower than that implied by the 5 GHz continuum

It should be mentioned here that the upper limits implied by the pulsar dispersion measure are not as rigorous as the TC5GHz

upper limits. This is because the contribution to the interstellar electron density from HII regions derived by Vivekanand and Narayan (1982) is an average over the entire galaxy. Therefore there could be large fluctuations in the average electron density from one line of sight to another. In addition, there was a scarcity of pulsars in the longitude range of our interest in the sample used by Vivekanand and Narayan (1982) for their analysis. Therefore it is possible that the average electron density of 0.02 cm^{-3} derived by them is an underestimate for directions with $\ell \lesssim 40^{\circ}$. Nevertheless, the implied upper limits gives us a feeling for the electron temperatures allowed by these considerations.

It is possible to set a lower limit to the electron temperture and therefore to the emission measure from geometrical considerations. In fig. 6.11 and 6.12 it can be seen that the observed intensities of the 166α and 272α lines require that EM and T_e be proportional to each other. A lower eletron temperature implies a lower emission measure which in turn implies a smaller effetive path length, as the density of the region is fixed. For a temperature of 100K, (which is the typical temperature of HI clouds) the implied path lengths are in the range of 0.2 - 2 pc.

As pointed out by Shaver (1976), with such small path lengths the geometry of these regions would be very peculiar. The scale height of this gas (z) is estimated to be $\sim$ 70-80 pc from a study of the lattitude extent of the 166α emission by Lockman (1976) and Hart and Pedlar (1976). Therefore this gas would have dimensions of $\sim$100 pc in the direction perpendicular to the line of sight. For low electron temperatures the above small effective path lengths implied, would require these regions to be in the form of thin extensive sheets or small cloudlets distributed along the line of sight with a very small filling factor. Both these geometries would be inconsistent with the smooth observed line profiles of width 30-50 kms^{-1}. The extensive sheet with its low temperature would produce a single strong narrow feature whereas the distributed

cloudlets would result in a number of weak narrow features extending over a large velocity range.

It is difficult to set any rigorous lower **limit** to the temperature from these geometrical considerations. However **it is** reasonable to expect that the path length be comparable to or larger than the lateral extent of the gas, which is or the order of 50-100 pc. This lower limit on the path length requires that the electron temperature be higher than a few thousand degrees. The lower **limits** to the temperature and EM based on a path length of 50 pc through the gas are given in Table 6.2.

It may be possible to set a lower **limit** to the electron temperature of the ionized region just from its electron density. This is because ionization always results in heating of the gas. In fact the main source of heating in most of the interstellar regions is through ionization after which the excess energy carried by the liberated electron is converted into kinetic energy of the particles through collisions **(Spitzer** 1978). The electron density of 1-10 cm^{-3} derived above for the blank regions implies high ionization rates for hydrogen. **It** may not be possible to achieve such electron densities without heating the gas to a considerable degree. We recall that an average of **0.5 eV** excess energy of the ionizing photons, over the 13.6 **eV** ionization potential would result in a kinetic energy of the electrons corresponding to temperature of $>$ **5000K.**

We conclude that the temperature of the gas responsible for the blank region lines is greater than a few thousand degrees. A discussion of the derived parameters will follow after the analysis of SNR directions. $\blacksquare$

6.4   IONIZED GAS TOWARDS SNRs

In general, radio recombination lines are not expected from supernova remnants **(SNRs).** In fact, in many cases the absence of recombination lines from a radio continuum source is used to identify **it** as a non-thermal **soure** or an SNR. Any recombination

line detected towards a known SNR is therefore attributed to ionized gas lying along the line of sight to the remnant.

In the present study, 272α line observations have been made towards 11 directions corresponding to 10 well known SNRs. Two of the adjacent directions observed (near W44) correspond to the same SNR. The positions and names of the SNRs observed are given in Table 5.1. The H272α line has been detected towards all the SNR directions observed. The line parameters are given in Table 5.2

Recombination lines at higher frequencies have been detected earlier towards at least 3 of these SNRs. Cesarsky and Cesarsky (1973a,b) have detected 92α, 166α and 157α towards 3C391 and 166α line towards W49B. Bignell (1973) has detected the 1666. line in the direction of W44. The 134α line towards W49B has been observed by Downes and Wilson (1974). The lowest frequency recombination line observed. so far has been that of Pankonin (1975) who detected the 248α line towards SNRs 3C391 and W49B.

Most of the above SNRs are in the galactic plane and have longitudes $\lt 50^{\circ}$. The above observations have indicated the presence of ionized gas along the line of sight to these sources. There is also further evidence for the presence of ionized gas in the direction of SNRs. This is in the form of a turnover in the continuum spectrum of these sources at low frequencies. Dulk and Slee (1972, 1975) have observed such a turnover towards some of these sources at 80 MHz. The turnover is attributed to free-free absorption by the line of sight ionized gas and they have estimated the continuum optical depth (τ_{80}) towards 14 SNRs.

The SNR directions are similar to the blank regions discussed in the previous section. The only difference is the presence of a strong background source in addition to the galactic non-thermal background. Therefore we can derive the electron density and set limits on the temperature and emission measure of the ionized gas responsible for the observed line,

using the same method as employed for the blank regions. For this purpose we shall use the high frequency recombination line measurements mentioned above and thse 80MHz optical depth reported by Dulk and Slee (1975).

6. 4. 1 Electron density of the gas

The observed 272α line parameters and the measured continuum temperature T_{BC} for nine of the SNR directions is given in Table 6.3. The parameters of the high frequency lines observed towards three of these diretions (3C391, W49B and W44) and the references are also given in Table 6.3. For the other 6 directions we use the 166α line parameters observed by Lockman (1976) or Hart and Pedlar (1976) at the nearest position. These parameters are also listed in the table. For 4 of these 6 positions the available 166α measurement is within the Ooty beam and for the other 2 positions they are within $0^\circ.4$ of the 272 beam centre. The measured value of the 80MHz optical depth, wherever available, is also given in Table 6.3.

The model described in Section 6. 3. 3 was used for deriving the density. The relevant background temperature T_0 is the sum of the contribution from the SNR and the galactic non-thermal background. This was estimated as follows.

We first estimated the expected average brightness temperature T_{BSNR} over the 2°x6' beam due to the SNR. This was done using the 408 MHz flux density, spectral index and size given in the catalogue of Clark and Caswell (1976). The contribution to the observed brightness temperature T_{BC} (given in Table 6.3) from the galactic non-thermal background was then taken to be

$$T_{Bg} = T_{BC} - T_{BSNR}$$

The effective temperature of the radiation coming from behind the cloud for each of the 9 directions was calculated as

$$T_0` = T_{BSNR} + T_{Bg}/2$$

TABLE 6.3 : Observed Parameters towards SNRs

Source	H2CO Line Parameters						High Frequency Parameters							
	V_{LSR} (km/s)	T_L (°K)	ΔV (km/s)	T_{BC} (°K)	T_{SNR} (°K)	T_O (°K)	Line (km/s)	V_{LiR} (km/s)	T_L (°K)	ΔV (km/s)	T_O (°K)	Ref	$T_a\gamma(8■)$ a- (°K)	T_c(5GHZ) (°K)
1	2	3	4	5	6	7	8	9	10	11	12	13	14	15
G357.7-0.1 ...	-7.9(1.3)	1.3(2)	40(3)	930	276	534	166α		0.027(18)		13.4(1.4)	1	0.12(25)	0.8
G6.6-0.1 W28	11(2)	1.1(2)	43(4)	900	284	592	166α		0.052(19)		16.7(1.2)	1	......	0.4
G11.2-0.3 ...	37(2)	0.8(2)	23(6)	760	189	475	166α		0.06		15.4	2	0.09(38)	0.4
G21.8-0.6 ...	54(2)	0.7(12)	44(5)	790	151	470	166α		0.038(14)		7.7(6)	1	......	0.4
G23.0-0.3 ...	68(2)	0.84(14)	55(4)	770	136	453	166α		0.058(14)		13.2(1)	1	......	0.6
G31.9+0.0 3C391	98(1)	0.9(2)	10(2)	680	181	431	92α 157α 166α	103 99.8 100	0.007 0.045 0.04	30 35 28	1 10.7 9	4 5 6	0.46(25)	0.4
G34.6-0.6 W44	48(1)	0.87(16)	21(3)	830	325	576	166α	50	0.036(09)	21	30	3	......	0.2
G39.2-0.3 3C396	84(2)	0.66(13)	21(5)	570	141	356	166α		0.017(12)		6.4(0.6)	1	0.02(09)	0.2
G43.2-0.1 W49	63(1)	1.2(2)	35(3)	690	315	503	166α 134α	60 65(10)	0.02 0.019(03)	30 45	.. 19	6 7	0.44(09)	0.2

References : 1. Lockman(1976), 2. Hart and Pedlar(1976), 3 Bignel(1973), 4 Cesarsky and Cesarsky(1973b), 5 Seacord(1975), 6. Cesarsky and Cesarsky(1973a).

where **it** is assumed that half of the observed background originates behind the cloud. The values of T_0 are given in Table 6.3. Since the galactic background is negligible at higher frequencies all of the observed continuum was assumed to originate behind the cloud i.e. the SNR. As in the case of blank regions we have used a beam dilution factor of 0.6 for the 2724 line and 1.0 for the high frequency lines. The respective widths of the lines at the two frequencies, wherever available, was used for the calculation. Otherwise, the observed 2724. line width was used for both low and high frequency lines.

The density for each of the source directions was obtained using the method described in section 6.3.4 for the blank regions, and using the parameters for the high and low frequency lines given in Table 6.3. The plot of emission measure as a function of N_e for different temperatures is shown in figures 6.13 and 6.14 for two SNR directions G357.7–0.1 and G31.9+0.0. As expected, the density N_e is almost uniquely given by these curves irrespective of T_e or EM. The density is given by the intersection of the 272α and the high frequency curve. The derived densities for all the directions are given in Table 6.4. These densities appear to be reliable within a factor of 2.

When more than one high frequency measurement was available for a given direction, as in the case of 3C391 and W49, we obtained the density in a similar way using each of the high frequency lines. The densities so derived were within a factor of I.5 of each other. The densities for all the SNR directions are in the range of 0.5–7 cm^{-3}.

6.4.2 <u>Electron temperature and Emission measure</u>

We can set limits to the temperature and emission measure using similar considerations as for the blank regions. With the density of the gas fixed as described above, a relationship between EM and T_e is established through the intensity of the 272α or the high frequency line. This is shown in figures 6.15 and 6.16, for the two SNRs G357.7–0.1 and 3C391.
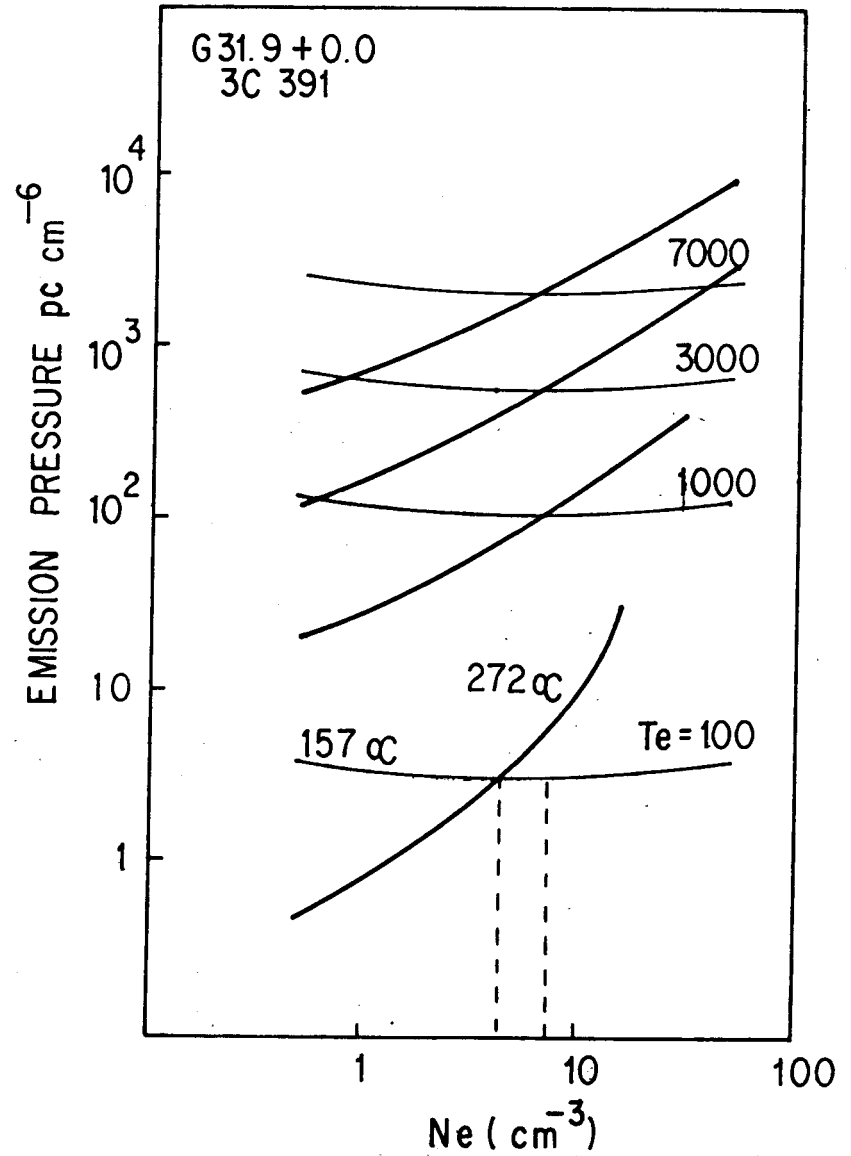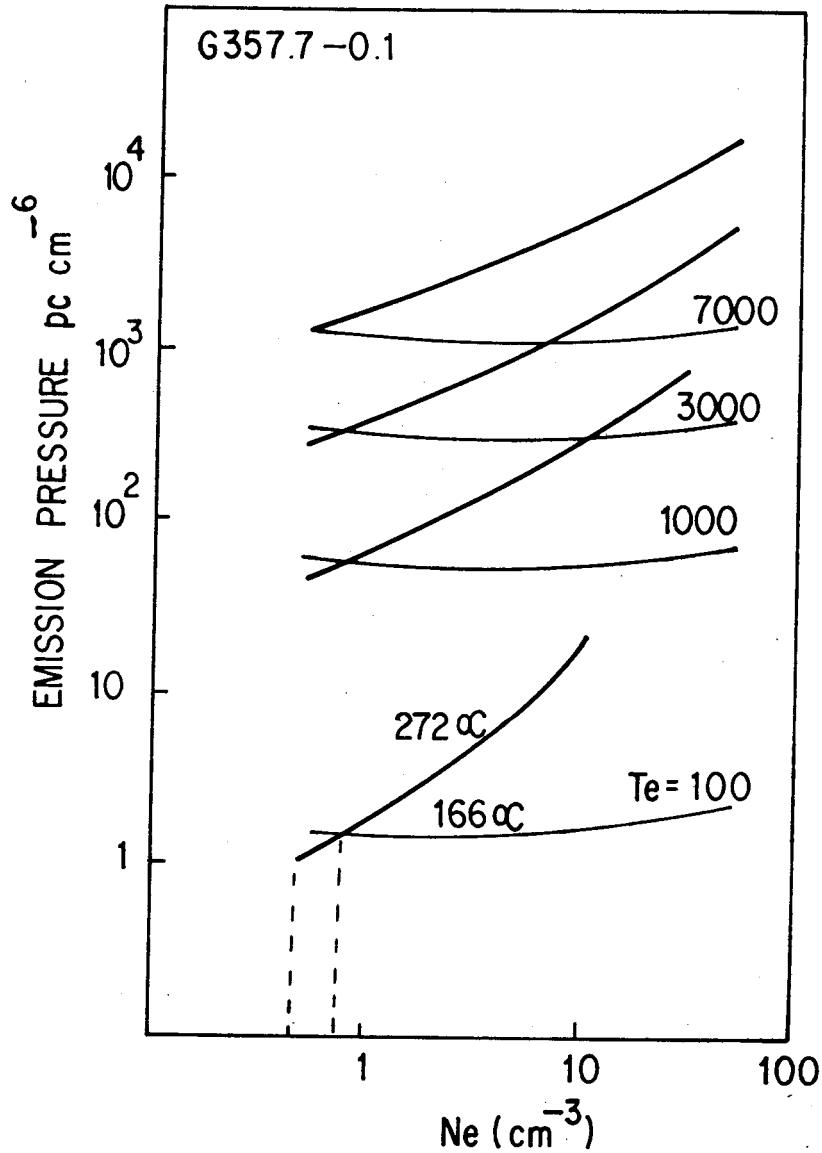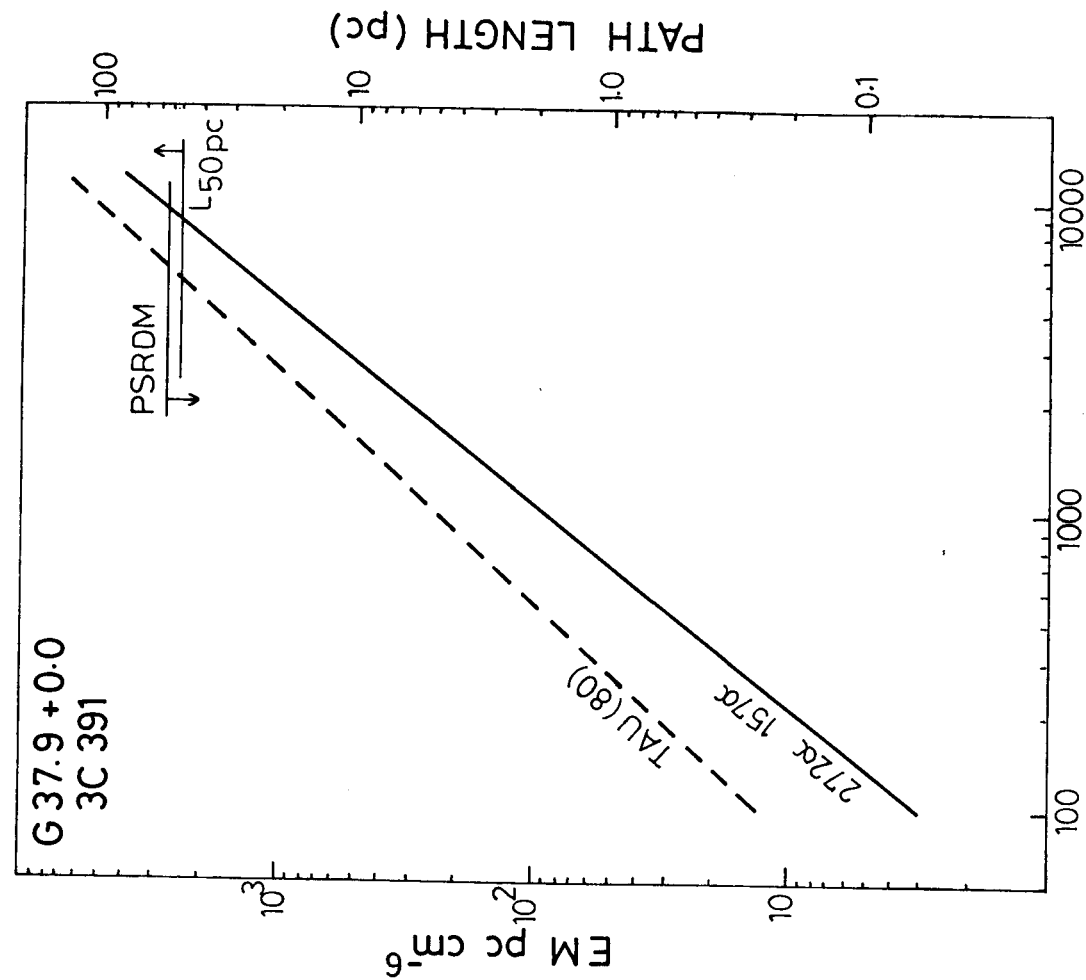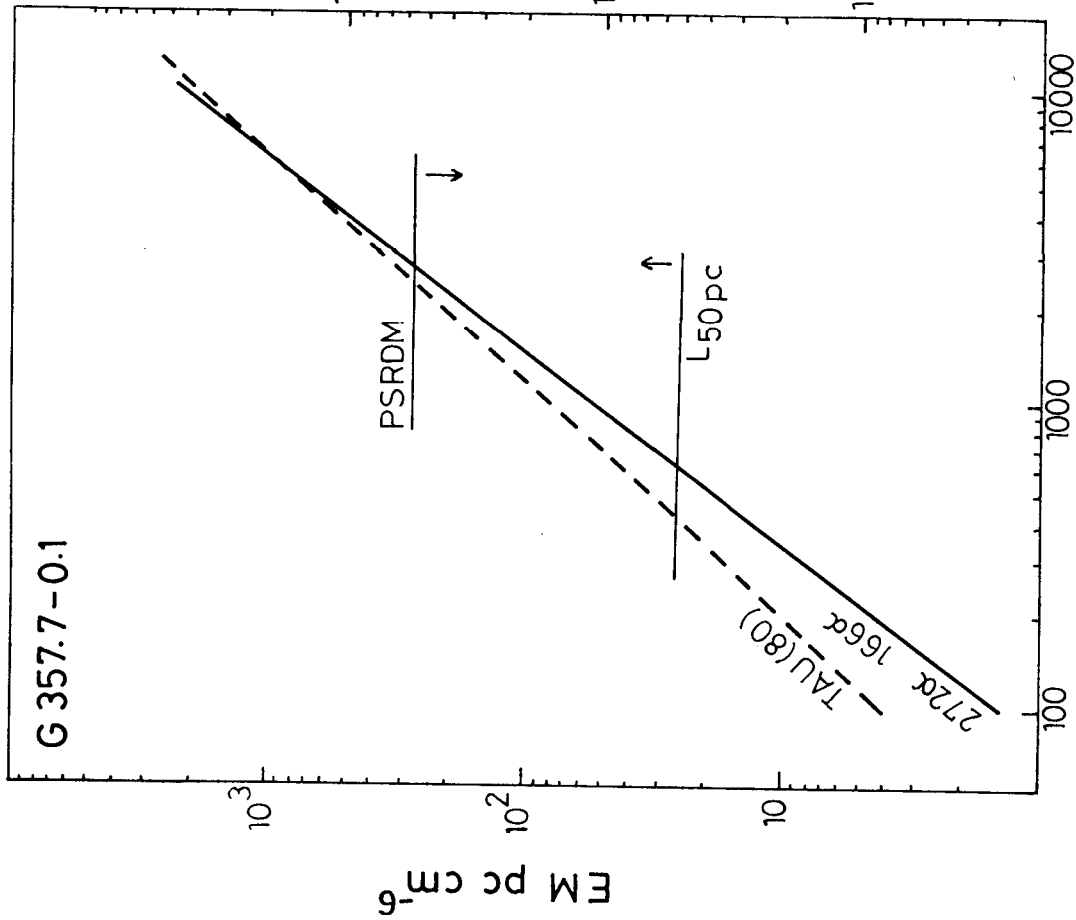
Fig. 6.13 and 6.14   Emission measure as a function of Ne, required to produced the H272α and the high frequency line towards 2 SNRs. The intersection of thick and thin lines give the density.

Figs. 6.15 Relationship between EM and T_e to produce the observed 272α and 166α line
and 6.16 intensities towards two SNRs. N_e is determined from figs. 6.13 and 6.14.
The limits implied by pulsar DM and pathlength are also shown (see text).

In the case of an SNR however, the 5GHz continuum cannot be used to set a upper limit on the electron temperature of the ionized gas along the line of sight. This is because, most of the observed continuum is emitted by the SNR it self.

The upper limits implied by the pulsar DM (eq. 6.4) are given in Table 6.4. As mentioned earlier, these upper limits are not rigorous.

To set lower limits to the temperature we have used the same geometrical considerations as for the blank regions. Namely the electron temperatures should not imply peculiar geometries inconsistent with the observed line profiles. The lower limits obtained by requiring that the path lengths through the gas be >50 pc, so that it will be comparable to the lateral extent of the region, are given in Table 6.4.

Although there is another measured quantity (τ_{80MHz}) pertaining to the ionized gas, along the line of sight to some of the SNRs (Dulk and Slee, 1975), it cannot be used to put an independent constraint on any of the parameters. This is because the continuum optical depth depends only on the emission measure and electron temperature ($\propto EM \times T_e^{-3/2}$) and is independent of density. If one requires that the ,gas produce all of the observed τ_{80} , the relation between EM and T_e is very similar to the corresponding relation for explaining the observed intensity of the 272α or 166α line. In Figures 6.15 and 6.16 the line marked τ_{80} represents this relation for the observed value of τ_{80} towards the sources G357.7-0.1 and 3C391 (Dulk and Slee, 1975). As can be seen, this line runs almost parallel to the lines marked 2724 and 166α. Therefore, even if all of the observed continuum optical depth is produced by the same gas from which recombination lines are observed, the value of τ_{80} cannot be used in conjunction with the line intensities to determine T_e or EM. However, one can require that the gas responsible for the recombination lines should not produce more than the observed 80 MHz optical depth. This is easily satisfied for all the SNR directions we have considered. The 80 MHz optical depth of' the

TABLE 6.4 : Properties of Ionized Gas Towards SNRs

Source	N_e cm^{-3}	Upper Limit form PSR DM			Lower Limit With L>50pc		Values for T_e= 5000		
		L pc	T °K	EM cm^{-6}pc	T K	EM cm^{-6}pc	EM cm^{-6}pc	L pc	Tau 9cMHz
G357.7-0.1	0.7	570	2500	280	700	25	700	1430	0.11
G6.6-0.1	2.5	160	4000	1000	2000	312	1300	208	0.21
G11.2-0.3	4	100	7000	1600	4500	800	850	53	0.14
G21.8-0.6	3.8	105	6000	1500	4000	722	1050	73	0.17
G23.0-0.2	4	100	5000	1600	3000	800	2000	125	0.33
G31.9+0.0	7	51	8000	2500	7000	2450	1200	25	0.20
G34.6-0.6	1.1	363	6000	440	1800	61	360	297	0.06
G39.2-0.3	0.7	570	5000	280	1500	25	300	612	0.05
G43.2-0.1	1.5	266	3000	600	1100	113	1000	44	0.16

recombination line emitting regions calculated with $T_e = 5000K$ are given in Table 6.4. (In this case τ_{eo} is almost independent of temperature since EM is related to T_e through the 2726 or 166α line intensity). It turns out that the line emitting regions can account for most of the observed 80 MHz optical depth.

6.5 DISCUSSION OF THE DERIVED PARAMETERS TOWARDS BLANK REGIONS AND SNRs

An examination of Tables 6.2 and 6.4 reveals that the parameters characterizing the ionized gas towards SNRs and blank areas in the galactic plane are quite similar. The regions responsible for the observed lines have densities in the range of 1 - 10 cm^{-3}, their temperatures are greater than a few thousand degrees but less than about 8000K, and they have emission measures of 500 to 2500 $cm^{-6}pc$. The corresponding path lengths through the gas are in the range 50 - 150 pc. The similarity is not surprising since the gas towards both these sets of directions (SNRs and blank regions) is the same as that responsible for galactic ridge recombination lines observed at centimeter wavelength. Any phenomena that is as widespread and uniform as the galactic ridge recombination lines must have some very general explanation. Obtaining the parameters of the gas responsible for the phenomena is just one step towards this goal.

The parameters derived here account for the observed strength of the galactic ridge recombination lines, and the high frequency recombination lines towards SNRs. This is necessarily true since we have made use of these lines to constrain the parameters. They account for most of the 80 MHz continuum optical depth observed by Dulk and Slee (1975). This gas can possibly also account for the background thermal emission seen in the galactic plane.

The parameter characterizing the gas responsible for the galactic ridge recombination lines and the lines towards supernova remnants have been a topic of discussion in the literature since the first observations by Gottesman and Gordon

(1970). We shall briefly review here some earlier work and compare our results with them. The initial attempts to acount for the galactic ridge lines were all directed towards explaining them as arising from the general interstellar medium Gordon and Gottesman (1971) suggested a diffuse medium with a temperature of ~1000K. Cesarsky and Cesarsky (1971) and Lockrnan and Gordon (1973) proposed that the lines originate in cold dense clouds in the interstellar medium Making use of the 80 MHz optical depth reported by Dulk and Slee (1972), the recombination line observed towards the SNR 3C391 was also interpreted by Cesarsky and Cesarsky (1973b) as arising in a cold cloud. All the cold cloud interpretations ran, in general into three difficulties. They implied high ionization rates in cold clouds in conflict with the theories of the interstellar medium (Field, Goldsmith and Habing 1969, Hjellming Gordon and Gordon 1969); the observed lines did not extend over the velocity range of 21 cm emission or absorption, and they could not account for the observed correlation between the continuum and line intensities (Mathews et al 1973, Jackson and Kerr 1975).

Subsequently, the observed galactic ridge lines have been interpreted in terms of hot gas presumably weak HII regions. Mathews et al (1973) separated the thermal continuum from the observed galatic background and together with their observed 166αline intensities estimated the temperature of the regions to be ~6000K. Jackson and Kerr (1975) also used a separation of the thermal continuum, but based on their observed correlation of the H110αline intensity with the total continuum, and arrived at a temperature of ~4500K.

Chaisson (1974) interpreted the recombination line towards the SNR 3C391 in terms of a line of sight HII region. Downes and Wilson (1974) also explain the recombination lines observed towards SNRs 3C391 and W49B as arising due to HII regions along the line of sight.

Shaver (1976) has made the most comprehensive study of the available data on the galactic ridge reombination lines and the

lines observed towards SNRs. Combining this data with the few low frequency (408 and 386 MHz) recombination line measurements, then available, (Pankonin et al 1974, Pankonin 1975, Gordon et al 1974) he has concluded that the lines arise in HII regions having electron densities 5-10 cm^{-3}, diameters of 20-100 pc and emission measures of 2000-4000 pc cm^{-6}. He has not quantitatively estimated the temperatures of these regions, but favours temperatures of the order of 5000K.

Lockman (1980) has analysed the 166α data near $1 = 36^{o}$ and concludes that the gas responsible for the line emission has a temperature of 1000K, an emission measure of a few hundred cm^{-6} pc and a density of $\sim 1 cm^{-3}$.

The parameters derived by us for the line emitting gas in the direction of SNRs and blank regions are consistent with an interpretation in terms of high-temperature, moderate-density 1 0 cm^{-3}) regions. Our results are very similar to those of Shaver (1976) who also used low frequency recombination lines for deriving the parameters. In fact the technique adopted by us is similar in many ways to that of Shaver (1976). Although we cannot quantitatively estimate the temperature of the gas, we also favour higher temperatures (a few thousand degrees) based on considerations of pulsar dispersion measure and geometry of the line emitting region.

Based on these results alone it is not possible to decide the origin of this gas. With the small path lengths of 50-150 pc derived for these regions they cannot be regarded as some component of the general interstellar medium; the average path length through the galaxy at these longitudes is 20 kpc. This gas could be in the form of a number of small HII regions, low density envelopes of bright HII regions seen in the galactic plane or some other kind of ionized gas produced in localized regions of the interstellar medium. We shall return to this question after the analysis of the lines observed towards HII regions. It will then be shown that most of the low frequency recombination lines arise in outer low density envelopes of

bright **HII** regions and that there are sufficient number of them in the inner galaxy ($\ell \leq 40°$) to account for most of the galactic ridge recombination lines and the lines observed towards supernova remnants.

6.6 LINES OBSERVED TOWARDS HII REGIONS

6.6.1 General considerations :

These are possibly the best studied ionized regions of the galaxy. They appear **as** prominent sources in the radio continuum surveys of the galactic plane **(e.g.** Altenhoff **et al** 1970, 1978, Haynes et **al 1978)** and are more numerous than any other type of galactic radio source.

A large number of **HII** regions have been studied using their continuum emission **(e.g.** Shaver and Goss **1970)** and also high frequency radio recombination lines (e.g. Reifenstein **et al** 1970, Wilson **et al** 1970, Downes **et al 1980).** Both continuum and lines have been used to determine their electron temperatures and generally only the continuum for their densities. From many such studies **it** is now known that **HII** regions have electron temperatures in the range 4000-10000K, electron densities in the range $10^{2} - 10^{4}$ cm^{-3} and emission measures of $10^{4} - 10^{6}$ pc cm^{-6}. Their linear sizes are generlly a few parsecs.

There are 30 such **'conventional'** HII regions towards which the H272 line has been detected in the present observations. The observed line intensity and width for 21 of these directions are given in Table 6.5. As mentioned in Section **5.3,** the intensity of the recombination line from these **HII** regions is expected to be very weak due to the effects of pressure broadening and beam dilution. As discussed in Section 6.2, we can set upper limits on the density of the gas responsible for the lines from the observed width alone. These upper **limits** for the electron density are given in Column 4 of Table 6.5.

TABLE 6.5: Optical Depth and Sizes of HII regions and Upper Limits on Density

Source		$T_L(272\alpha)$ (°K)	ΔV (km/s)	$N_{e_{max}}$ (cm^{-3})	$N_{e_{mn}}$ (cm^{-3})	T_e (°K)	EM (cm^{-6} pc)	Tau at 325MHz	size (')	Beam Dilun.
1		2	3	4	5	6	7	8	9	10
G2.3+0.2		0.48(12)	18(5)	20		3700	4.2E+04	0.6	3.6	0.005
G4.4+0.2		0.39(09)	66(13)	90		5700	6.7E+04	6.5	4.2	0.006
G6.0-1.2	M8	1.1(0.2)	43(4)	50	370	7700	3.4E+05	2.0	4.5	0.006
G7.0-0.3	M20	0.63(13)	30(6)	30	143	7500	7.7E+04	0.4	5.7	0.008
G8.1+0.2		0.64(12)	47(7)	60		6500	4.7E+05	3.0	2.9	0.004
G10.2-0.3	W31	0.77(13)	51(4)	65	356	5700	1.0E+06	7.0	3.1	0.004
G12.8-0.2	W33	0.72(13)	32(4)	35	1774	7900	4.8E+06	23.0	0.8	0.001
G14.0-0.1		1.0(2)	38(3)	45		5800	8.4E+04	0.6	3.3	0.005
G15.1-0.7	M17	0.67(12)	41(5)	50	581	9100	1.8E+06	7.0	9.1	0.076
G16.9+0.7	M16	0.73(11)	53(3)	70		6100	6.9E+04	0.5	8.1	0.067
G20.7-0.1		0.45(11)	19(6)	15	96	5900	7.4E+04	0.5	4.5	0.006
G24.8+0.1	W42	1.0(15)	77(4)	100	51	5800	2.8E+04	0.2	5.0	0.007
G25.4-0.2	3C385	0.49(10)	77(15)	100	224	7100	2.9E+05	2.0	3.2	0.004
		0.27(10)	26(11)	30						
G27.3+0.2		0.98(16)	85(6)	120		7400	8.6E+04	0.4	2.9	0.004
G28.8+3.5	W40	0.27(05)	35(4)	40	273	8500	1.2E+05	0.5	5.8	0.008
		0.36(06)	44(4)	55						
G29.9+0.0		1.0(20)	35(4)	40	>111	6100	1.7E+05	1.0	4.3	0.006
G30.8+0.0	W43	1.2(20)	41(3)	50	205	6000	5.2E+05	4.0	5.5	0.008
G35.1-1.6	W48	0.61(11)	55(6)	70	>20	7250	1.5E+04	0.08	5.3	0.007
G37.8-0.2	W47	0.31(09)	33(11)	35	>130	8400	5.8E+04	0.3	2.9	0.004
		0.76(09)	49(7)	60						
		0.68(09)	17(3)	5						
G49.0-0.3	W51B	0.86(11)	23(4)	10	87	9000	1.2E+05	0.5	7.0	0.058
G206.0-2.1	W16	0.4(10)	28(5)	20	18	6000	8.6E+03	0.06	55	0.46

Parameters for the HII regions are taken from the high frequency' measurements of Shaver and Goss (1970b), Silverglate and Terzian (1979) Viner et al (1979) and Downes et al (1980)

Most of these HII regions have been studied elsewhere using both the continuum and high frequency recombination lines. The electron density, temperature and emission measure obtained from such studies, if they are available, are given in Columns 5, 6 and 7 of Table 6.5. From a comparison of Columns 4 and 5 of this table, it is clear that with the exception of one or two sources, the HII regions themselves cannot be responsible for the lines observed here. Column 8 of the table shows that most of these HII regions are optically thick at our frequency and for this reason too they are unlikely to produce the observed recombination lines. Further, for most of these sources the beam dilution factor is $10^{-2} - 10^{-3}$ (column 10) due to the 2° x 6' antenna beam used in these observations which is much larger than the few arcminute sizes of these sources (column 9). The beam dilution will reduce the intensity of the already weakened lines (due to pressure broadening and optical depth) to practically undetectable levels. Therefore, the observed H272α lines in these directions must arise in some gas other than the HII regions.

On the other hand, the above arguments are not applicable to any high frequency recombination lines (even the 166α). Pressure broadening is virtually absent and the HII regions will still be optically thin at these frequencies; coupled with the better angular resolutions (5-20 arcminutes) available, this implies that observations at higher frequencies ($>$1GHz) can easily detect recombination lines from these HII regions.

This being so, it is not possible to use the same technique as used for the blank regions and SNR diretions to obtain the density of the gas responsible for the observed H272α lines. It is pratically impossible to separate the contribution of this gas to the observed line intensity at high frequencies from that of the HII region itself.

However, since the location of the HII region in most of these cases is known from the high frequency recombination line velocities, and 21cm HI absorption measurements (e.g.

Radhakrishnan et al 1972), the first comparison to make is the location, with respect to the HII region, of the gas responsible for the 272α lines as implied by the observed velocities. In column 3 of Table 6.6 we have given the observed velocity of the 272α line and in Column 4, that of a high frequency line (in most cases the H110α line at 4.87 GHz observed by Downes et al 1980). There is generally a very good agreement between the two velocities, particularly if we take into account the width of the observed lines. In all the cases the 272α line emission is seen at the velocity of the high frequency line. This immediately implies that the lower density gas responsible for the 272α line is associated with the HII region. Clearly, the low density gas can only be the .outer envelopes of the dense HII regions responsible for the observed high frequency recombination lines and the continuum

The picture that emerges therefore is that the HII regions which are prominent in the continuum (having densities of $10^2 - 10^4$ cm^{-3}), and which produce most of the observed high frequency recombination lines, have low density envelopes which can give rise to low frequency recombination lines. The high density cores make practically no contribution to the low frequency lines. It would be difficult to separate the contribution of the low density envelope to high frequency recombination lines; the intensity of the high frequency lines will in fact be dominated by the emission from the high density cores.

There is both theoretical justification and observational support for the above picture. In a classic paper Brocklehurst and Seaton (1972) showed that in orde'r to explain the observed line to continuum ratio as a function of frequency it is necessary to use models of HII regions which contain extensive outer regions of low density. Hart and Pedlar (1976) have observed 166α line emission from 13 positions near the HII region W3 and conclude that there is an extended low density region assoiated with this object. Theoretical justification for models with low density outer regions will be discussed later.

TABLE 6.6 : Velocity, Background Temp. and Derived Parameters of HII regions

Source	T_{BG} $(°K)$	V_{LSR} 2724 (km/s)	V_{LSR} 110α (km/s)	Dist (kpc)	T_C $(°K)$	Derived Parameters		
						N_e cm^{-3}	EM cm^{-6}pc	L pc
1	2	3	4	5	6	7	8	9
G2.3+0.2	750	9 (2)	5	...	375	...	....	...
G4.4+0.2	700	4 (5)	5.7	17.0	350	1.8	1100	356
G6.0-1.2	660	-4 (1)	3.0	1.4	660	15	7000	29
G7.0-0.3	720	6 (2)	14	1.5	720	7.5	1700	31
G8.1+0.2	770	25 (3)	22	...	770	...	....	...
G10.2-0.3	610	15 (2)	13	9.0	300	3.6	2800	188
G12.8-0.2	730	26 (2)	30	4.4	730	4	1500	92
G14.0-0.1	680	24 (2)	31.5	4	680	4	1600	84
G15.1-0.7	810	9 (2)	11.5	2.4	810	8	3000	50
G16.9+0.7	610	20 (1)	28	2.2	610	7.5	2600	46
G20.7-0.1	590	47 (3)	57	13.8	300	1.1	380	290
G24.8+0.1	660	83 (2)	107	9	330	4	3500	186
G25.4:0.2	650	54 (6) 107 (5)	59	13.2	340	2	1100	276
G27.3+0.2	640	93 (2)	33	15.2	320	4	4800	318
G28.8+3.5	450	72 (2) 19 (2)	0.7	0.7	450	15	3500	15
G29.9+0.0	650	91 (2)	98.5	9	330	3.5	2500	189
G30.8+0.0	830	95 (1)	90	7.1	830	3	1500	149
G35.1-1.6	460	34 (3)	43	3.2	460	7	3500	67
G37.8-0.2	480	0.3 (5) 44 (3) 87 (1)	61	11.5	250	4.8	5500	241
G49.0-0.3	690	61 (2)	60.5	6.6	690	3.1	1400	138
G206.0-2.1	100	5 (2)	7 (3)	1.4	0	11	4000	29

Distances are taken from Downes et al (1980) or Radhakrishnan et al (1972)

Based on such a model, we shall now derive or put constraints on the parameters of the low density regions from the observed intensity of the 272α line.

6.6.2 Electron temperature of the low density envelopes

The temperature of low density envelopes of HII regions is unlikely to be very different from that of the cores. As discussed in Section 2.1 the temperature of a fully ionized region is basically governed by the abundance of heavy elements like Oxygen, Nitrogen, Neon etc. The electron temperature depends only weakly on the effective temperature of the exciting star or stars and the density of the gas. Since the core and the outer envelope were presumably parts of the same cloud the abundance of heavy elements in them is unlikely to be very different. If the exciting star for the outer envelope is embedded in the core, then a case can be made for the outer envelope to be at a somewhat higher temperature. This is because there will be a hardening of the radiation emerging after ionization of the core, which will on the average impart a slightly higher kinetic energy to the electrons liberated in the outer regions. On the other hand, the lower density in the outer regions can slightly reduce the collisional de-excitation of the coolant ions (OII, OIII etc) thereby increasing the efficiency of the cooling process. The actual temperature will therefore depend on the relative importance of these two processes. If the exciting star is in the outer region itself, then only the second argument applies and the resulting temperature can be somewhat lower than that of the core.

For our purposes, it is reasonable to assume that the electron temperature of the low density envelope is essentially the same as that of the core. These temperatures for each of the HII regions is given in column *6* of Table *6*.5. Most of these temperatures are derived from the H110α measurements of Downes et al (1980), on the assumption of LTE.

6.6.3 Electron density and Emission measure:

We have used an isothermal, uniform density model similar to the one used for the case of blank regions and SNR directions. The model is illustrated in Fig. 6.17. The difference here is that the high density core of the HII region is embedded inside the low density region responsible for the 272α line. This can have two effects. The continuum radiation from the core can cause stimulated emission of the recombination line in the lower density gas in front of it. Secondly, if the core is optically thick at this frequency, then it can block the line emission originating from behind it. However, the angular sizes of these HII regions (~5 arcmin) are very small compared to the 2^0 x 6' beam used for the observations, and therefore their contribution to the continuum temperature is, in most cases, negligible compared to the non-thermal galactic' background which is nearly uniform over the beam. We can therefore neglect to first order both the above effects.

The expected line brightness temperature is given by

$$T_{BL} = (\Omega_s / \Omega_B) \, T_L$$

where (Ω_s / Ω_B) represents the beam dilution for the low density region. If T_0, T_N, T_e, N_e and EM are specified for the line emitting region, then T_L can be calulated using the equation (2.77). For all of the HII regions, their kinematic distances are known from their high frequency recombination line velocities. For most of these HII regions, the distance ambiguity has been resolved using either 21 cm HI absorption meaurements (Radhakrishnan et al 1972) or formaldehyde absorption in their direction (Downes et al 1980). The distances are given in Table 6.6.

For nearby HII regions, the background temperature T_0 was taken to be equal to the observed continuum brightness temperature T_{BC} listed in Table 6.6. For those HII regions which are known to be at the far kinematic distance, T_0 was calculated using

$$T_0 = (T_{BC} - T_{H\bar{u}})\, h \qquad T_{H\,II}$$
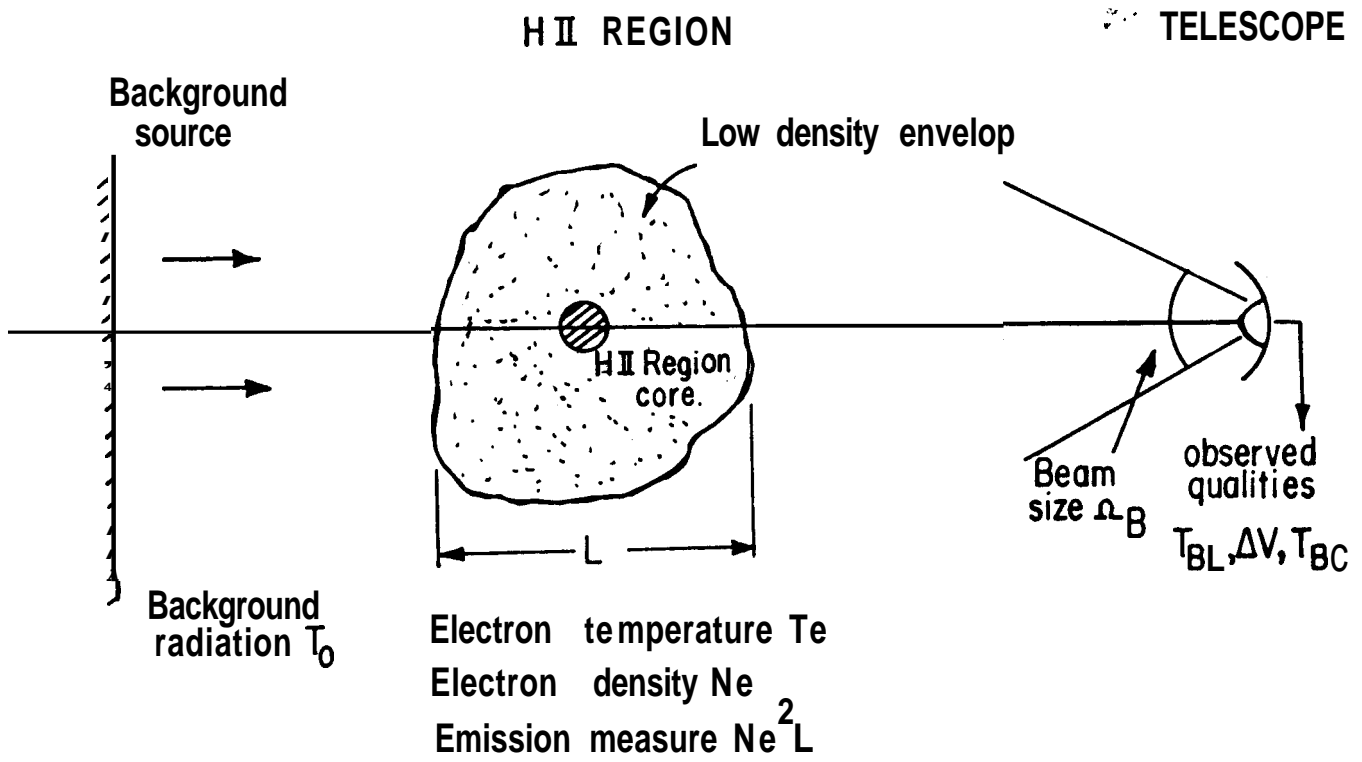
FIG.6 17 MODEL   FOR   INTERPRETING   LINES   OBSERVED
TOWARDS H II REGIONS.

where T_{HII} is the beam averaged brightness temperature of the **HII** region core calculated using its T_e, N_e, **EM** and its angular size θ derived from high frequency measurements (See Table 6.5). In the case of the **HII** region W16 (the Rosette nebula) we have used $T_o = 0$ since it is in the anticentre direction. In addition this source is known to be a low density $(10-15 \text{ cm}^{-3})$ large angular size source $(\sim 1^{\circ})$; therefore the observed 272 line can originate from the **HII** region itself. We have used $T_N = 0$ for all the cases.

We have calculated the emission measure required, for densities in the range $0.1 - 100 \text{ cm}^{-3}$, to produce the intensity of the 272α recombination line observed towards each of the 19 **HII** regions. We have used the electron temperatures derived from high frequency measurements (Table 6.5). The calculations were done using beam dilution factors of 0.3 and 0.6. The dilution factors are unlikely to be much outside this range since the latitude extent of the 166α line emission observed in the galactic plane by **Lockman** (1976) and Hart and Pedlar (1976) is about $\pm 0^{\circ}5$. The above calculations were not carried out for 11 of the 30 **HII** regions (towards which H272α line was detected) either because the velocity did not match with that of the high frequeny line, or the distance to the **HII** region was not known.

The results of these calculations are shown for four of the **HII** regions (M20, M16, 3C385 and W43) in Figures 6.16 to 6.21. The two curves marked 272α(0.3) and 272α(0.6) in each of these figures shows the required emission measure, as a function of electron density, to produce the observed 272α line intensity, when the beam dilution factor is 0.3 and 0.6 respectively.

The density and emission measure can be any where within this range provided they satisfy the relation between them implied by the above **EM** vs N_e curves. We therefore need another constraint on either of these parameters to determine both of them As mentioned earlier, we cannot use the parameters of the high frequency lines observed in the same direction since they will be dominated by emission from the central core. If careful
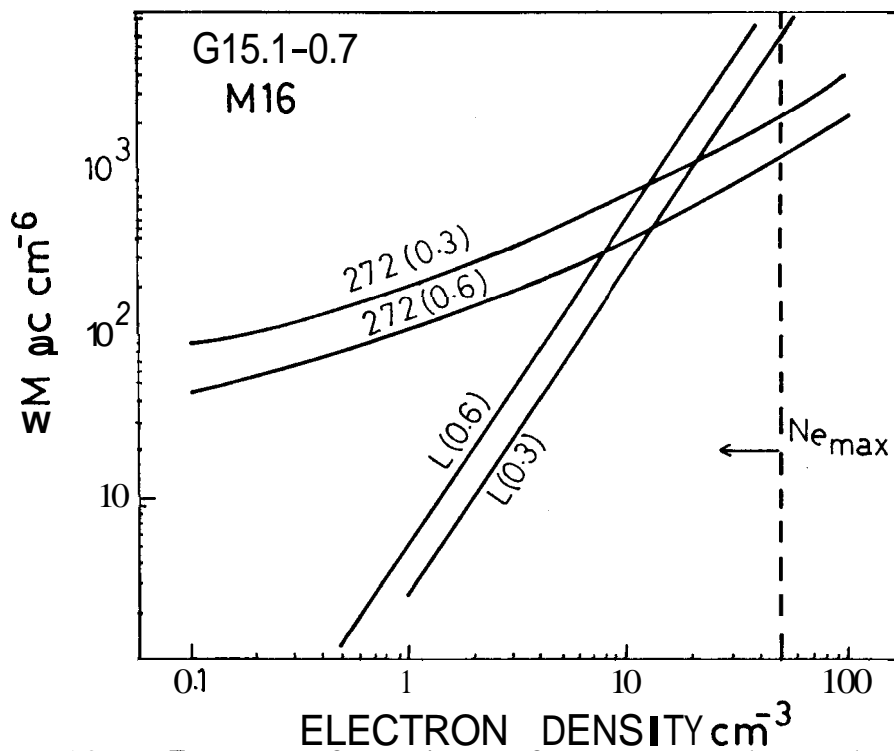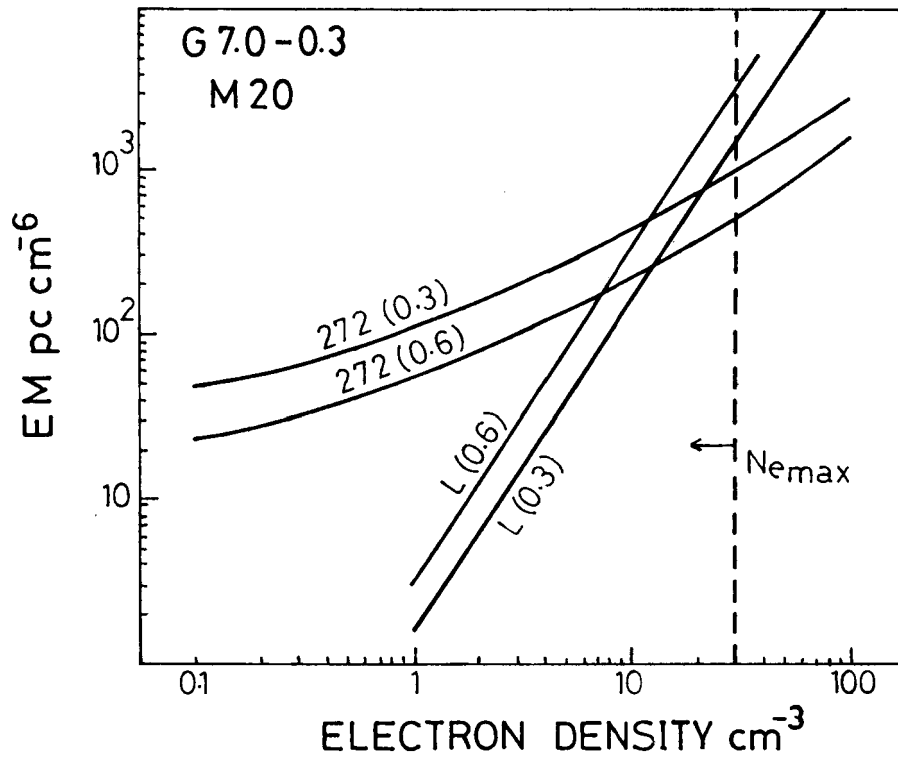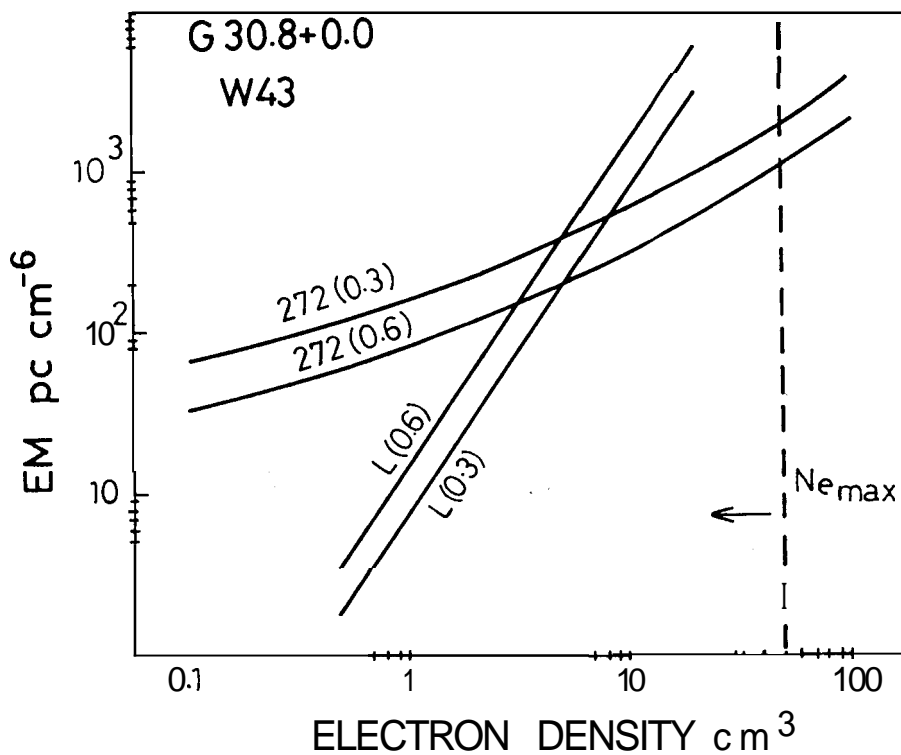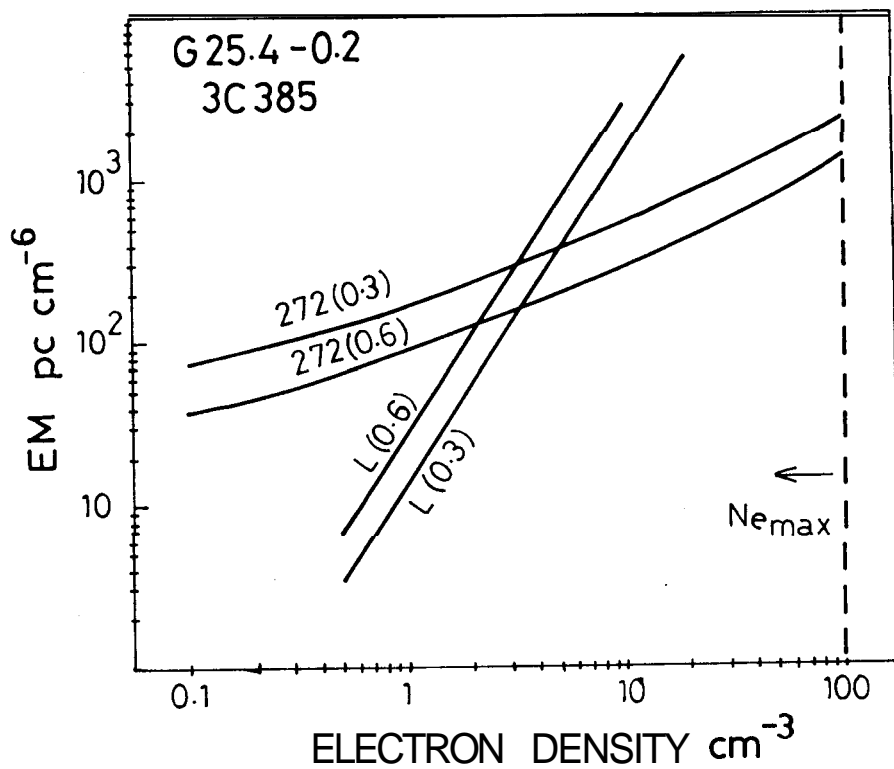
Fig. 6.18   EM as a function of N_e to produce the observed H272α
and 6.19   line intensity towards 2 HII regions. The lines
marked L indicates the restriction due to geometry
(see text). The numbers in brackets are the beam
dilution.   Upper limit on N_e from pressure broadening
is also indicated.

Figs, 6.20   **Same** as **figures** 6.18 and 6.19 for two other
and 6.21   HII regions.

measurements are made at high frequencies away from such cores using a narrow beam, then **it** would be possible to use them together with the above calculation to derive both the electron density and emission measure, as also the electron temperature. Such a measurement towards one such ontinuum minimum region (near $\ell = 24°.1$) has in fact been made by **Mebold et al** (1976). But unfortunately none of our beam positions overlap with their observed direction.

Under the circumstances, we use here what we consider a reasonable constraint based on geometrical considerations. The assumed beam dilution factor (supported by the angular extent of the 166α line emission) implies an angular size of $0°.6$ to $1°.2$ for the line emitting regions (the low density envelopes). This combined with the known distance to the source will lead to a linear size for the envelope perpendicular to the line of sight. It. is reasonable to assume that the extent of the envelope **along** the line of sight is comparable to its linear size in the perpendicular direction.

We thus impose the restriction that the emission measure and electron density of the gas be related by

$$EM = N_e^2 \, L_\perp \qquad (6.7)$$

where $L_\perp$ is the **size** of the line emitting region perpendicular to the line of sight given by

$$L_\perp = d \cdot D \cdot \Theta_\alpha \qquad (6.8)$$

where is the distance to the HII region, $\Theta_\alpha = 2°$ is the east-west beam of the telescope, and D is the beam dilution factor. **The** region is assumed to fill the beam in the north-south direction (**i.**e. the angular extent of the gas is $>6'$).

The two inclined straight lines marked **L(0.3)** and **L(0.6)** in each of the figures 6.18 to 6.21 shows the above restriction on the density and emission measure of the region for beam dilution **fators** 0.3 and 0.6 respectively. The intersection of these lines

with the corresponding curves marked 272 (0.3) and 272 (0.6) define the emission measure and electron density of the envelope from which the 272α line is observed. As mentioned earlier, the beam dilution factor D is unlikely to be outside the range of 0.3 to 0.6 for most of the cases. $D > 0.6$ would imply the latitude extent of the gas to be $|b| > 0.7-0.8$ if we take into acccount the offset of $0.1 - 0.2$ from $b = 0$ of the HII regions observed here. This would be inconsistent with the latitude extent of the 166α recombination line emission observed by Hart and Pedlar (1976) and Lockman (1976). For most of the sources analysed here, when $D < 0.2$ was used the solution obtained from the intersection of the curves such as in Figures 6.18 to 6.21 implied densities N_e which were much greater than allowed by the observed width of the lines. This is beause the curve marked 272α moves upwards and the line marked L moves to the right as the dilution factor D is decreased.

The electron density, emission measure and the path length through the gas obtained assuming the most probable beam dilution factor of 0.6, are given in Table 6.6. If the dilution factor D is greater than 0.6 by some factor, then the derived densities will be lower by nearly the same factor. The densities are in the range $1 - 10$ cm^{-3}, emission measures are in the range $1000 - 4000 cm^{-6} pc$ and the corresponding path lengths through the regions are 30-300 pc. The temperatures of these are assumed to be the same as those of the cores which are in the range 5000-9000K.

6.6.4 Discussion of the derived parameters

The density and emission measure derived by us for the gas responsible for the observed 272α recombination lines towards HII regions are about a factor of 10-100 (in most cases more like 100) less than that of conventional HII regions. There are only a very few low frequency recombination line observations towards HII regions available in the literature to compare with our results (e.g. Gordon et al 1974, Pankonin et al 1974, Parrish[4] et al 1977 and Pedlar et al 1978). There are 4 HII regions

common to our survey and the 386 MHz observations of Gordon et al (1974), but these authors have not attempted to derive the physical parameters of the region responsible for the lines. Parrish et al (1977) interpreting their 300 MHz observation towards W51B find that this line arises in a region of density <30 cm^{-3} and has an angular size ~ 25 arcmin. They also argue that this low density gas is associated with the discrete source W51B, due to the observed similar velocities of high and low frequency lines. This in fact is the argument we have used as a starting point for deriving the parameters. Pedlar et al (1978) interpret their low frequency observations towards the galactic centre in terms of low density gas with $N_e \sim 10$ cm^{-3}. They note that any single component model requires that, the electron density be ~ 10 cm^{-3} (irrespective of EM and T_e) to account for the low frequency lines towards the galactic centre. All these results are quite consistent with the parameters derived by us.

There is at least one HII region (W16, the Rosette nebula) in our survey which is known to be large and of low density for which we can diretly compare the parameters derived by us with those from high frequency measurements. We obtain a density of 11 cm^{-3} and EM of 4000 pc cm^{-6} which are consistent with the parameters ($N_e = 9$ cm^{-3}, EM=2600 pc cm^{-6}) derived by Pedlar and Maws (the 1973) using the 166α line and by Viner et al (1979) ($N_e = 16$ cm^{-3}) using the H100α recombination line.

A comparison of the parameters for the low density envelopes of conventional HII regions derived here and those for the regions responsible for the observed lines towards blank regions and SNRs derived in the previous sections (Tables 6.2 and 6.4) reveals that they are very similar. As the lines observed towards SNRs and blank regions are attributed to the gas responsible for the galactic ridge recombination lines, the above similarity immediately suggests that the latter may also arise in low density extended envelopes of HII regions seen in the galactic plane. We shall pursue this suggestion further in the next chapter where it will in fact be shown that most of the galactic ridge recombination Lines do arise in the extended

envelopes of conventional HII regions prominent in the radio continuum surveys. HII regions are so numerous in the inner part of the galaxy that given the kind of low density envelopes suggested by the analysis in the previous section, they intersect practically every line of sight in the galactic ridge having $\ell \leq 40°$, thereby giving rise to recombination lines in every direction within this range.